Salinomycin disturbs Golgi apparatus function and specifically affects cells in epithelial-to-mesenchymal transition

Running title: Salinomycin impairs Golgi function

Marko Marjanović[a,c,d], Ana-Matea Mikecin Dražić[a,c], Marija Mioč[a, e], Mladen Paradžik[a,f], Filip Kliček[b], Mislav Novokmet[b], Gordan Lauc[b] and Marijeta Kralj[a,g,*]

[a] Division of Molecular Medicine, Ruđer Bošković Institute, Bijenička c. 54, 10000 Zagreb, Croatia

[b] GENOS, Glycoscience Research Laboratory, Borongajska c. 83, 10000 Zagreb, Croatia

[c] These authors contributed equally

[d] ORCID: 0000-0001-9850-0561

[e] ORCID: 0000-0001-5290-6945

[f] ORCID: 0000-0003-1025-5595

[g] ORCID: 0000-0002-7165-2722

*Corresponding author: +385 1 4571290, marijeta.kralj@irb.hr

Abstract

Epithelial-to-mesenchymal transition (EMT) gives rise to cells with properties similar to cancer stem cells (CSCs). Targeting the EMT program to selectively eliminate CSCs is a promising way to improve cancer therapy. Salinomycin (Sal), a K^+/H^+ ionophore, was identified as highly selective towards CSC-like cells, but its mechanism of action and selectivity remains elusive. Here we show that Sal, similarly to monensin and nigericin, disturbs the function of the Golgi apparatus (GA). Sal alters the expression of GA-related genes and leads to marked changes in GA morphology, particularly in cells that underwent EMT. Moreover, GA disturbing agents severely affect post-translational modifications of proteins, including protein processing, glycosylation, and secretion. We discover that the alterations induced by GA disturbing agents specifically affect the viability of EMT cells. Collectively, our work reveals a novel vulnerability related to the EMT, suggesting an important role for the GA in the EMT, while targeting the GA represents a novel therapeutic approach against CSCs.

Summary Statement

We show that salinomycin impairs the morphology and function of the Golgi apparatus and blocks proper posttranslational modification and sorting of proteins, to which EMT cells are particularly susceptible.

Keywords

EMT, breast CSCs, Golgi apparatus, ER, salinomycin, monensin, N-glycosylation

Introduction

Epithelial-to-mesenchymal transition (EMT) is a cell transdifferentiation program during which cells lose epithelial characteristics (e.g. adhesion and lack of motility) while they acquire a mesenchymal phenotype associated with cell migration (Nieto and Cano, 2012). Epithelial carcinoma cells that have passed through the EMT show properties of cancer stem cells (CSCs), which includes invasiveness, drug-resistance and the ability to form metastases at distant organs. Thereby the EMT contributes to cancer metastasis and relapse (Shibue and Weinberg, 2017). Hence, targeting the EMT program to selectively eliminate CSCs is a promising way to improve cancer therapy (Nimmakayala et al., 2019; Pattabiraman and Weinberg, 2014).

It was demonstrated that the induction of the EMT in immortalized human mammary epithelial cells (HMLEs) results in the expression of stem cell markers and the acquisition of the breast CSC phenotype. Consequently, these cells have been established as an experimental cell model of CSCs (Gupta et al., 2009; Mani et al., 2008). High-throughput screening of a large compound library on the HMLE cell model identified several drugs selective towards EMT/CSCs. The most potent compound was salinomycin (Sal), a potassium ionophore widely used as a coccidiostat (Gupta et al., 2009). Many subsequent studies proposed potential mechanisms of Sal's selectivity against CSCs, as well as pursuing specific vulnerabilities of EMT and CSCs (Antoszczak, 2019; Kaushik et al., 2018; Pattabiraman and Weinberg, 2014; Wang et al., 2021)

Up to date, Sal has been shown to affect tumor cells through various mechanisms including activation of apoptosis, autophagy, and elevation of intracellular ROS, as well as mitochondrial membrane depolarization, and inhibition of multidrug resistance pumps. Moreover, several studies have used Sal to potentiate the efficacy of other commonly used anticancer chemotherapeutics (Antoszczak, 2019; Dewangan et al., 2017; Huczynski, 2012; Kaushik et al., 2018; Managò et al., 2015; Shi et al., 2015). Nevertheless, despite the enormous efforts in the past decade, the specific mechanism of Sal's EMT/CSC selectivity remains vague. Recently, Huang et al. showed that Sal accumulates in the ER and thus promotes the release of Ca^{2+} into the cytosol. This leads to the unfolded protein response (UPR) and activation of CHOP which inhibits Wnt signalling, an effect already ascribed to Sal in CLL (Huang et al., 2018; Lu et al., 2011).

It was demonstrated that the ER-mediated UPR is permanently activated in EMT cells to support synthesis and secretion of large quantities of extracellular matrix (ECM) proteins. Hence, ER function is critical for EMT cells' maintenance, offering a new therapeutic approach (Feng et al., 2014). In addition to increased secretory output, the EMT process involves major cellular remodelling including changes in membrane lipidome characteristics and reduced membrane fluidity, which is needed for migration and invasion (Kalluri and Weinberg, 2009; Sampaio et al., 2011). Distribution of both the proteins and the lipids inside the cell is dependent on the functionally intertwined

communication between the ER and the GA (Smirle et al., 2013). In addition, Mai et al. demonstrated that derivatives of Sal localize in lysosomes causing accumulation of iron and activation of ferroptosis as the main mode of CSCs cell death (Mai et al., 2017). Since Sal affects most membrane-enclosed cellular compartments, especially the ones involved in protein production, modification and secretion, as well as the fact that some ionophores with CSC selective abilities belong to the GA inhibitors (Dinter and Berger, 1998; Kaushik et al., 2018), prompted us to examine the significance of the GA in EMT cells and its sensitivity to Sal. In the present study, we demonstrate that Sal affects the GA morphology as well as the expression of ER-Golgi related genes predominantly in EMT cells. Moreover, we show that Sal inhibits correct GA function which leads to altered post-translational protein modifications that are specifically processed in the GA. These include reduced secretion of proteins and marked changes in the N-glycosylation profile of secreted proteins, primarily diminishing the amount of complex N-glycans. Since our data undisputedly positions Sal as a Golgi disturbing agent and because EMT cells demonstrate greater sensitivity to the GA perturbations, we propose that targeting of the GA is a novel therapeutic path against EMT cells, and consequently against CSCs.

Results

EMT sensitizes cells to salinomycin and monensin

A seminal study by Gupta et al. (Gupta et al., 2009) identified four highly selective compounds against EMT cells: abamectin, etoposide, nigericin, and salinomycin. In addition, the screening process resulted in the discovery of an additional 32 selective compounds. We conducted a similar analysis on the same data set from Gupta et al., using the same algorithm but with a more permissive threshold. Our analysis revealed a total of 227 selective compounds, including several ionophores or ionophore-like molecules (see Methods for details; Supplementary file S1A). Among these, the most interesting compound was monensin (Mon), which was experimentally confirmed as a potent EMT-selective cytotoxic compound in a prostate cancer model (Vanneste et al., 2019) (Supplementary file S1B).

In the current study, we took the advantage of the same EMT models used by Gupta et al. (Gupta et al., 2009), in which non-EMT cells (HMLE-shGFP and HMLE-pBp) express epithelial marker E-cadherin and have $CD24^{high}/CD44^{low}$. Conversely, EMT cells (HMLE-shEcad and HMLE-Twist) express N-cadherin as well as $CD24^{low}/CD44^{high}$ (Fig. S1A–C). We confirmed that Sal lowered the proportion of EMT cells in a mixed population experiment (Fig. 1A and S1D). Sal also showed a more pronounced effect towards EMT cells in proliferation assays (Fig. 1B and C). The observed selectivity diminished at higher concentrations of Sal (5 µM for shEcad/shGFP or 10 µM for Twist/pBp pair) which were toxic

for both EMT and non-EMT cells. Higher concentration also resulted in immediate loss of mitochondrial potential, which was even more pronounced in HMLE-pBp (non-EMT) cells, possibly explaining the loss of selectivity (Fig. S1E). This proved its selectivity against EMT cells, although to a lesser extent than previously described (Gupta et al., 2009). Finally, Mon also displayed selective growth inhibition of EMT cells and enriched the percentage of cells with epithelial markers in a mixed population experiment (Fig. 1A–C, S1D). The effect was comparable to Sal. Conversely, paclitaxel (a negative control) enriched the EMT population, corroborating published data (Gupta et al., 2009) (Fig. 1A and S1F). Thus, our data clearly demonstrate that Mon exhibits EMT-selective inhibition not only in the prostate model, as reported previously (Vanneste et al., 2019), but also in the breast EMT cell model (HMLE). This confirmation of results in different models underscores the consistent efficacy of Mon as an EMT-selective agent.

To test selectivity more generally, particularly in breast cancer cell lines, we examined the influence of Sal and Mon in a broader range of cell lines distinguished by their epithelial or mesenchymal phenotype (Figure 1 D). We used the cell line MCF -7, which is non-metastatic and represents the luminal subtype of breast cancer, and the cell lines SUM 159 and MDA-MB -231, both basal B-cell lines known to be metastatic. Basal breast cancer cells were found to have a higher propensity to undergo EMT and express the CSC markers (Feng et al., 2014; Zhao et al., 2016). In addition, we used HCT116 and HepG2 colon and liver cancer cells, respectively. Both cells exhibited an epithelial phenotype and were reported previously to be more resistant to treatment with Mon (Vanneste et al., 2019). The results confirmed that both Sal and Mon similarly affected the viability of these cell lines and confirmed that the cell lines with epithelial properties - MCF -7 and HCT116 - were the most resistant, whereas MDA-MB -231 and SUM 159 cells were significantly more sensitive. In contrast to the results of Vanneste et al., HepG2 cells showed higher sensitivity, comparable to SUM 159 cells.

The results reported previously (Vanneste et al., 2019) also suggest that Mon uptake correlates positively with cell sensitivity status. To test whether Sal selectively accumulates in HMLE EMT cells, we performed LC-MS/MS analyses to quantify the amount of Sal in lysates of HMLE-pBp and HMLE-Twist cells exposed to 0.2 and 5 µM Sal for 24 hours. Our results show no statistical difference in Sal uptake between EMT and non-EMT cells after treatment with 5 µM Sal (Fig. 1SG). When incubated with 0.2 µM Sal, the intracellular concentration either fell below or was near the detection limit. This result led to considerable variability between measurements, making it difficult to draw definitive conclusions (data not shown).

Overall, our data confirmed that Sal and Mon, similarly to nigericin (Nig) are EMT-selective agents. They are structurally similar polyether ionophores with preferences for monovalent ions. It is

noteworthy that Mon and Nig are known Golgi-disturbing agents, a property not previously attributed to Sal.

Figure 1. EMT sensitizes cells to salinomycin and monensin. (A) HMLE-Twist and HMLE-pBp were seeded on day 0 at 1:1 ratio and then treated with salinomycin (Sal), monensin (Mon) or paclitaxel (PTX) at indicated concentrations. Ratio of $CD44^{high}/CD44^{low}$ (EMT/non-EMT) cells after 3 days of treatment of mixed culture is shown. Representative CD24/CD44 flow cytometry profiles are shown in the right panel. (B) Dose-response curves of HMLE-Twist (orange, EMT) and HMLE-pBp (dark blue, non-EMT) or (C) HMLE-shEcad (purple, EMT) and HMLE-shGFP (blue, non-EMT) breast cells treated with Sal (upper panels) and Mon (lower panels). (D) Dose-response curves of MCF-7, MDA-MB-231, SUM 159, HCT116 and HepG2 cells treated with Sal (left panel) and Mon (right panel). MTT assay was performed after 72 hours of treatment. Data are presented as mean ± s.d., n = 3 from duplicates in A and n = 3 from quadruplicates in B, C and D.

Salinomycin induces the expression of ER-Golgi related genes

To evaluate the effects of Sal on intracellular compartments, we profiled the global gene expression in both EMT and non-EMT cells by RNA-Seq. We treated HMLE-Twist and HMLE-pBp cells for 24 hours with a low concentration of Sal (0.2 μM), which showed the highest selectivity in both EMT models (Fig. 1A and S1D). The analysis of differentially expressed genes (≥ 2 fold change) revealed that: *i*) a common set of 52 genes were upregulated in both cell lines, *ii*) one gene (*NFE2L3*) was upregulated in EMT but downregulated in non-EMT cells, and *iii*) 3 genes (*IDI1*, *TM7SF2*, and *INSIG1*) were downregulated in EMT cells, but upregulated in non-EMT cells (Fig. S2A and Supplementary file S2A). We further widened the analysis for the case (*ii*), which yielded 64 genes (*ii+*; ≤ 0 in non-EMT and ≥ 2 fold change in EMT cells, Fig. S2B, and Supplementary file S2B). Both sets (*i* and *ii+*) include multiple genes related to the ER, the GA and membrane function, suggesting that Sal affects these cellular compartments predominantly. The observed effect can be considered either as a general mechanism of Sal (i) or as specific to EMT cells (*ii+*). Moreover, Gene Ontology (GO) analysis of these 2 gene sets showed enrichment of the secretory pathway-related genes (Supplementary file S2C and D, respectively).

We have additionally performed GO analysis on full sets of differentially expressed genes in the 3 experimental cases (EMT vs non-EMT, EMT with Sal and non-EMT with Sal). The analysis demonstrated that Sal treatment enriched for genes related to the ER and the GA regardless of the cell type which reinforced the notion that Sal enriches for genes involved in the secretory pathway (Fig. 2A). Additionally, a gene set enrichment analysis (GSEA) demonstrated that Sal significantly induced the expression of genes known to be upregulated by well-known GA stressors (monensin,

nigericin, brefeldin A and 4MU-xyloside) or which activate the ER-related UPR (tunicamycin and thapsigargin) (Fig. 2B and C, S2C). Sal also upregulated genes reported to be enriched upon the induction of the GA-specific UPR (Serebrenik et al., 2018) (Fig. 2B and C). On the contrary, we observed no enrichment for the gene set upregulated by the treatment with the DNA damaging chemotherapeutic doxorubicin (Fig. 2B and C). In addition, Sal also induced genes involved in glycosylation, a post-translational protein modification mainly executed inside the ER-GA compartments (Fig. 2C and S2C).

Figure 2. Salinomycin induces the expression of ER-Golgi related genes. RNA-seq analysis was performed on HMLE-pBp and HMLE-Twist cells (non-EMT and EMT) treated with or without 0.2 µM Sal for 24 hours in biological triplicates. Differentially expressed genes were sorted from highest to lowest in each of 3 experiments indicated and the list was analyzed with GOrilla algorithm (http://cbl-gorilla.cs.technion.ac.il/) for enrichment of cellular component (A) and biological process (D) GO categories. Names and codes for cellular component GO categories enriched in both HMLE-Twist and HMLE-pBp cells after treatment with Sal are indicated in red (A). (B) GSEA analysis for gene sets of known Golgi stressors monensin and nigericin, induction of unfolded protein response in Golgi (HyT36), ER stressor thapsigargin, DNA damage compound doxorubicin and GO category glycosylation on RNA-Seq data from HMLE-Twist cells treated with Sal is presented (analysis was performed on data ordered from largest to smallest) (see Methods for details about gene sets used). (C) Summary of GSEA analysis on different gene sets (ER and GA stressors or GO category) and their relation to enrichment in our experimental model (see Methods for details). * - significantly enriched; yellow - enrichment in mock treated sample, blue - enrichment in Sal treated sample. (D) Venn diagram for overlapping categories is shown with number indicating different GO categories. Biological processes GOs that were most enriched after Sal treatment in HMLE-Twist and HMLE-pBp cells are indicated in red and blue, respectively.

Importantly, the analysis also revealed the difference between EMT and non-EMT cells in response to Sal. While GO enrichment analysis of EMT cells showed enrichment of processes related to the ER, GA, ion transport, extracellular matrix organization and regulation of cell adhesion, the GO categories with the highest enrichment in non-EMT cells were related to the metabolism of alcohol, cholesterol, and lipids (Fig. 2D and Supplementary file S2E–G). Moreover, because genes upregulated in non-EMT cells and downregulated in EMT cells (set *iii*) are either directly involved in (*IDI1* and *TM7SF2*) or regulate (*INSIG1*) cholesterol biosynthesis, we assessed the global effect of Sal and Mon on cellular lipid content. We stained cells with Nile Red, a dye which can differentiate between neutral lipids (cholesterol ester or triglycerides) found in lipid droplets (LDs) (Diaz et al., 2008). We

found that both compounds increased green to yellow fluorescence, representing LDs with high cholesterol content, exclusively in non-EMT cells, agreeing with the gene expression data. On the other hand, there was no obvious change observed in EMT cells (Fig. S2D). In addition, EMT cells were reported to maintain low cholesterol to allow increased membrane fluidity necessary for migration and invasion (Sampaio et al., 2011). ABCA1, a cholesterol efflux transporter, is highly expressed in EMT cells and it was demonstrated that can be downregulated by anti-metastasis drugs including salinomycin (Zhao et al., 2016). Our RNA-Seq data confirmed increased expression of *ABCA1* in EMT cells (3.45 fold change) and Sal did decrease its expression in both cell lines. Taken together, observed data suggests that Sal targets cellular compartments involved in protein and lipid processing and secretion (the ER and the GA) which activate different gene responses in EMT and non-EMT cells.

Salinomycin affects Golgi apparatus morphology and leads to the activation of PERK branch of UPR

Next, we decided to investigate the effect that Sal has on the secretory pathway, namely the GA and the ER, as well as the induction of UPR. We inspected the GA morphology by confocal microscopy, using common GA markers GM130 and GIANTIN that co-localize with cis-Golgi and cis- to medial-Golgi matrix membranes, respectively. Sal induced fragmentation of Golgi cisternae, which appeared as a dispersed area within cells that stained positive for both GM130 and GIANTIN (Fig. 3A and B). The extent of the GA perturbations in EMT cells was statistically significant when compared to mock-treated cells (Fig. 3C and D). On the other hand, the GA of non-EMT cells did not display perturbations in morphology after Sal treatment. Of note, the dispersal of Golgi cisternae in un-treated non-EMT cells was on average much larger than in EMT cells ($p < 0.001$ for both markers, unpaired two-tailed T-test), but the variance within the populations was very large (Fig. 3C and D). More prominent GA fragmentation in EMT cells was also observed when cells were treated with Mon (Fig. 3E).

To test the effect on GA morphology in other cells, while overcoming the cytotoxic effects observed at higher concentrations of Sal, a model cell line was used to allow monitoring of Golgi morphology over time. HeLa cells stably expressing the trans-Golgi marker GalT-GFP and H2B-mCherry were treated with Sal at a concentration of 5 µM, live cell fluorescence microscopy was performed, and Golgi morphology was compared with untreated cells. Remarkably, a significant fragmentation of the Golgi apparatus (GA) was observed within only two hours after treatment with Sal, as shown in Supplementary Movies 1 and 2.

Figure 3. Salinomycin affects Golgi apparatus morphology and leads to the activation of PERK branch of UPR. Representative confocal microscopy images of HMLE-Twist and HMLE-pBp cells after

treatment with Sal for 24 hours. Cells were stained with anti-GM130 primary and secondary Alexa Fluor 568 antibodies (red, A) or anti-GIANTIN primary and secondary Alexa Fluor 488 antibodies (green, B). DNA was counterstained with DAPI (blue). Quantification of the total area of GM130 (C) or GIANTIN (D) positive organelle and the area of the nucleus of each cell was divided and plotted. Box plot charts plotted from n = 57, 52, 72, 61, 71 and 61 cells (from left to right) from 2 individual experiments. (E) Representative confocal microscopy images of HMLE-Twist and HMLE-pBp cells after treatment with tunicamycin (5 μg/mL) or monensin (5 μM) for 24 hours. Cells were stained as in A and B. (F) Western blot analysis of UPR related proteins: phosphorylated-eIF2α (p-eIF2α), total eIF2α, and CREB-2 (Atf4) proteins in HMLE-Twist and HMLE-pBp after treatment with 0.2 μM Sal for 24 hours. Tunicamycin was used as a positive control. Naphtol blue staining of transferred proteins was used as to evaluate equal loading. (G) RT-PCR analysis of UPR-related splicing of XBP1 in HMLE-Twist and HMLE-pBp after treatment with Sal for 24 hours. Tunicamycin was used as a positive control. GAPDH was used as a loading control. Maximum projection of 10 slices is displayed. Scale bar = 10 μm. One-way ANOVA with post-hoc Dunnett's multiple comparison test was used for statistical analysis (**$p < 0.01$, ***$p < 0.001$).

We also examined the status of the compartments between the ER and the GA, by staining the cells with antibodies for ERGIC53 and β'COP, markers of ER-Golgi intermediate compartment (ERGIC) and COPI retrograde vesicles, respectively. The microscopy confirmed that these compartments were also affected by Sal treatment and that EMT cells showed greater alterations, which were more evident on COPI vesicles (Fig. S3A).

Moreover, we also inspected Golgi morphology after treatment with tunicamycin, an early blocker of N-glycosylation that is a well-known inducer of the ER stress and UPR, and was shown to be selective against EMT cells (Feng et al., 2014). Tunicamycin led to a severe GA compaction only in EMT cells while its effect on GA morphology in non-EMT cells was negligible (Fig. 3E). Nevertheless, it induced UPR in both cell lines (Fig. 3F and G). It was previously shown that Sal can induce ER-stress and activate UPR (Xipell et al., 2016; Yoon et al., 2013), which we confirmed in our cell model. We observed the activation of PERK but not IRE1 axis of UPR signalling cascade (Fig. 3F and G). In a recent publication, it was also shown that a fluorescent conjugate of Sal accumulates in the ER and leads to a massive release of the ER-stored Ca^{2+} into the cytosol in JIMT-1 cells (~600% increase), which was proposed as its mechanism of action (Huang et al., 2018). This prompted us to examine changes in cytosolic calcium in our experimental model. In contrast, we observed minimal or no increase of cytosolic calcium after treatment with both Sal and Mon (5 and 0.2 μM, respectively) in our EMT model (Fig. S3B–D). Surprisingly, even thapsigargin, an inhibitor of sarco/endoplasmic

reticulum Ca^{2+} ATPase (SERCA) that leads to depletion of the ER calcium storage, led to an increase of only 60%. Although our results differ from published data, we acknowledge that there may be factors contributing to the observed discrepancy. One possible explanation is that HMLE cells are not as susceptible to a strong release of Ca^{2+} compared with other cell lines. A recent study by Lebeau et al (Lebeau et al., 2021) supports this notion and shows that Ca^{2+} release varies moderately after treatment with Th in different cell lines. Nevertheless, our collective results highlight the significant induction of stress in the GA by Sal, particularly in EMT cells, which showed increased sensitivity to the drug compared with non-EMT cells.

Salinomycin affects post-translational modifications and sorting of proteins

The Golgi apparatus serves as the central component of the secretory pathway, and it is the main site for the modification and sorting of the membrane and secreted proteins (Morré and Mollenhauer, 2009). Thus, we investigated the fate of membrane proteins after inducing the GA stress with Sal. Classical cadherins (e.g. E- and N-) have prodomain sequences (~130 a.a.) that guard the adhesive domains against interaction before they are activated by proteolytic processing. These sequences are cleaved off by an endoprotease in the late Golgi (Koch et al., 2004). Sal, as well as Mon and nigericin, led to the appearance of an additional band with a higher molecular weight of the EMT marker N-cadherin in western blot analysis. The effect was more prominent with a lower concentration of Sal (0.2 µM, Fig. 4A and S4A) and was observed from 24h through 72h after treatment (Fig. S4B). The same effect was observed in breast tumor cell lines with high proportion of CSC-like cells (SUM 159; Fig. 4B). Conversely, paclitaxel did not disturb proteolytic cleavage of N-cadherin corroborating the hypothesis that the consequence of Sal treatment is a GA stress-related effect. We confirmed incomplete proteolytic processing by using an N-cadherin prodomain specific antibody (Fig. 4C). Strikingly, although E-cadherin maturation also requires removal of its prodomain, the treatment with ionophores did not lead to an appearance of an additional protein band in non-EMT cells (Fig. 4A and B, S4A and B). Additionally, the E-cadherin expression increased after the treatment, especially with 5 µM Sal or 0.2 µM Mon (Fig. 4A and B).

In addition to altered processing, we observed higher mobility of membrane proteins N-cadherin, EGFR (epidermal growth factor receptor) and TFRC (transferrin receptor) in all treated cell lines (Fig. 4A and B). We hypothesized that Sal also alters glycosylation as the ER and the GA are the major sites of protein glycosylation, a most abundant post-translational modification of membrane and secreted proteins (Varki et al., 2009). Hence, to examine the effect of reduced glycosylation of N-cadherin, we treated protein lysates with PNGase F that removes glycans attached to proteins at Asn residues (N-glycosylation). Since PNGase F removes all N-linked sugars, mobility of N-cadherin was even greater than after Sal treatment, suggesting that Sal hindered N-glycosylation (Fig. 4D).

We also examined the effect of the GA stressors on protein secretion. We have specifically measured the amount of interleukin-8 (IL-8), a cytokine secreted by both cell types (non-EMT cells secrete higher amount of IL-8 than EMT cells (Low-Marchelli et al., 2013). Both Sal and Mon decreased the secretion of IL-8 by 40% or more in both cell lines (Fig. 4E).

Figure 4. Salinomycin affects post-translational modifications and secretion of proteins.
(A) Western blot analysis of membrane proteins N- and E-cadherin; epidermal growth factor receptor and transferrin receptor (EGFR and TFRC) in HMLE-shEcad and HMLE-shGFP breast cells (A) or three different breast tumor cell lines (B) that were treated for 24 hours with indicated concentrations of DMSO (Mock), salinomycin (Sal), nigericin (Nig), monensin (Mon) or paclitaxel (PTX). Naphtol blue staining of transferred proteins was used to evaluate equal loading; bloting of E-cadherin in (B) was performed after N-cadherin on the same membrane and it is showing in SUM159 cells, protein bands denoted by #. (C) Western blot analysis of proN-cadherin with specific N-cadherin prodomain antibody in HMLE-Twist cells after treatment with Sal for 24h. (D) Western blot analysis of proN- and N-cadherin in HMLE-Twist cells after treatment with PNGase F. (E) HMLE-Twist and HMLE-pBp cells were treated with DMSO (mock), salinomycin (Sal) or monensin (Mon) for 24 hours and media above cells was subjected to ELISA analysis of secreted IL-8. Data was normalized to mock-treated sample.

Next, we examined the fate of E- and N-cadherins after treatment with a competitive inhibitor of O-glycosylation (1-benzyl-2-acetamido-2-deoxy-(α)-D-galactopyranoside (GalNAc(α)-O-bn), a known GA stressor (Miyata et al., 2013), alone or in combination with Sal. As expected, treatment with GalNAc(α)-O-bn prevented O- linked glycosylation of N-cadherin and therefore decreased the molecular mass of the mature protein (Fig. S4C). Exposure to Sal and GalNAc(α)-O-bn resulted in both modifications and the mobility of both the N-cadherin prodomain and the mature protein was even greater than after treatment with Sal. On the other hand, neither the mobility nor the processing of E-cadherin was affected in non-EMT cells by GalNAc(α)-O-bn. However, the combination treatment reduced the expression and decreased the molecular mass of the mature protein to some extent. It is also noteworthy that treatment with GalNAc(α)-O-bn in combination with Sal or Mon additionally decreased the proportion of EMT cells in a mixed population experiment compared with Sal alone and showed a more pronounced effect on EMT cells in proliferation assays, whereas treatment with GalNAc(α)-O-bn alone had no effect (Fig. S4D).

In addition, we tested the effect of another compound known to disrupt Golgi apparatus function and organization by inhibiting protein transport from ER to GA, brefeldin A (BFA), together with the ER stressors tunicamycin and thapsigargin on N-cadherin and E-cadherin processing (in EMT and non-EMT cells, respectively) (Fig. S4E). Not surprisingly, tunicamycin inhibited N-linked glycosylation and therefore decreased the molecular mass of mature proteins in both EMT (N-cadherin in HMLE-Twist) and non-EMT cells (E-cadherin in HMLE-pBP and MCF -7 cells). Thapsigargin led to the appearance of an additional band with a higher molecular mass, indicating inhibition of prodomain processing in both non-EMT and EMT cells. On the other hand, surprisingly, BFA also resulted in an additional band, but only in non-EMT cells, i.e., the prodomain of E-cadherin, with no effect on glycosylation, whereas it inhibited only the glycosylation of N-cadherin, which was observed as a protein with a smaller molecular mass in EMT cells. A similar effect of thapsigargin and BFA in MCF -7 cells has been described previously (Geng et al., 2012), but their different effects in EMT cells have not been described yet. These results suggest that the same treatment modality has different effects in different cell models.

Our experiments on dose-dependent cytotoxicity against EMT and non-EMT cells revealed that BFA exhibited a significant decrease in the proportion of EMT cells in the HMLE cell model during a mixed population experiment. This selective effect on EMT cells was further confirmed in proliferation assays (Fig. S4F and G), supporting its selectivity. Previous studies have also demonstrated the ability of BFA to reduce stem cell potential and migration in breast cancer cells (Tseng et al., 2014). However, when we tested dose selectivity on a broader range of cell lines, the pattern observed for BFA differed from that observed for Sal or Mon. SUM 159 cells showed the highest sensitivity, whereas MCF -7 and MDA-MB -231 cells showed comparatively lower sensitivity. This discrepancy in the activity of BFA, Sal, and Mon in EMT and non-EMT cells may be due to differences in mechanisms and sites of action; BFA inhibits the transport of secreted and membrane proteins from the ER to the GA, whereas Mon acts in the medial to trans cisternae of GA. In addition, cell type-specific sensitivity to BFA has been previously demonstrated (Dinter and Berger, 1998; Rosa et al., 1992).

Furthermore, we investigated the effect of bafilomycin A, another stressor known to induce acidification of lysosomes, endosomes, and secretory vesicles, and which is commonly used to detect Golgi-associated posttranslational changes in proteins. In contrast to previous findings, we did not observe selectivity in the HMLE cell model (Fig. S4H and I), and there was a divergent effect on other cell lines. These results indicate a significant difference compared to the effects of Sal, Mon, and BFA, potentially due to distinct mechanisms of action (Dinter and Berger, 1998).

Overall, our experiments showed that Sal interferes with posttranslational modification of proteins, glycosylation, and protein secretion, aligning with the effects observed with Mon and to some extent with BFA, thus confirming Sal as a GA stressor.

Salinomycin and monensin suppress synthesis of complex N-glycan structures

We decided to examine the N-glycome of secreted proteins for two reasons. First, we hypothesized that Sal also functions as a glycosylation inhibitor considering the observed effects on the GA, similarly to Mon, an established inhibitor of glycosylation (Dinter and Berger, 1998). Second, as EMT cells were shown to depend profoundly on the increased protein secretion (Feng et al., 2014), we also hypothesized that not only diminished secretion but also a change in glycosylation of secreted proteins negatively affects EMT cell maintenance and thus represents the underlying mechanism of selectivity of these compounds. Analysis of the secretome, in comparison to the complete proteome, allowed us to overcome possible masking by uncompleted glycan structures of proteins undergoing the process of glycosylation in the cellular compartments.

The major glycan structural features in EMT and non-EMT cells were mostly similar, with both having a similar distribution of N-glycan types (oligomannose, hybrid and complex), similar relative amounts of fucosylated structures and structures with higher branching (Fig. 5A–E). Moreover, the secreted N-glycomes of both EMT and non-EMT cells comprised of primarily complex-type N-glycans (>80%). We also found one paucimannose structure (peak 3). However, relative ratios of specific glycan structures were dramatically different resulting in N-glycome profiles specific for each cell line (Fig. S6). This difference was expected because of different expression profiles between EMT and non-EMT cells and thus the different composition of secretomes. Besides, it was demonstrated that breast cell lines exhibit specific N-glycosylation signatures of their secretomes relative to their tumorigenic level and breast cancer subtype (Lee et al., 2014).

After chromatogram integration, we defined 33 distinct chromatographic peaks in EMT and 30 peaks in non-EMT cells (Fig. S5 and Tables S2 and S3). The N-glycan structures present in each peak were determined by HILIC-UPLC-FLR-MS/MS approach. Many peaks contained more than one glycan structure, but in most cases, one single structure was the most abundant (i.e. the major structure; Tables S2 and S3, and Supplementary file S3). Glycan profile of EMT cells was dominated by 3 peaks (14, 16 and 20) that represented 39.3% of the total chromatogram. On the other hand, the glycan profile of non-EMT cells was dominated by 4 peaks (16, 17, 19 and 20) representing similarly 39.2% of the total glycome profile. Major glycans found in peaks 16 and 20 from HMLE-Twist cells matched to major glycans found in peaks 16, 17 and 19, 20 from HMLE-pBp cells (FA2G2S1 and FA2G2S2, respectively; Fig. S5D and Tables S2 and S3). Further, EMT cells lacked terminal fucosylation reflecting the fucosyl transferases' expression. In addition, EMT cells had reduced total relative amount of

sialylated glycans in comparison to non-EMT cells. Besides, sulfated or phosphorylated N-glycans (S/P) were found only in EMT cells, which had 4 such structures forming individual peaks 17, 21, 28 and 32 (Fig. 5A–E, S5, and Tables S2 and S3).

Treatment with either Sal or Mon had a drastic impact on N-glycosylation of secreted proteins in both cell lines. Strikingly, the effect of these two ionophores was extremely similar. Detailed analysis showed that each observed change was in the same direction and of similar potency when compared to mock-treated samples (Fig. 5A–E, S5B–D, and Tables S2 and S3). Thus, as treatments with both ionophores produced N-glycome profiles that were hardly distinguishable, we will mainly discuss treatment vs. control regarding glycosylation. The differential effect of the treatment between cell lines was marginal (Fig. 5A and S5D). Treatment did not completely abolish N-glycosylation of secreted proteins. Rather, it mostly blocked the processing of larger and more complex N-glycan structures as the relative amount of these glycans was significantly reduced in both cell lines. In turn, this led to a relative increase of simple, oligomannose-type N-glycans structures, reflecting the semi-stalled glycosylation machinery (Fig. 6A and S6D). Moreover, an increase in oligomannose structures after treatment is indicative of GA rather than ER -specific action, because mannoses are formed at ER. Therefore, a decrease in oligomannose structures would be expected if the treatment is ER -specific. A similar phenotype was observed on all structures that appear with increased N-glycan complexity. For instance, we observed decreased total sialylation, with especially affected tri-/tetra-antennary sialylated structures; decreased branching and decreased fucosylation of the N-glycome (Fig. 5B–E). These findings demonstrated that Sal and Mon disturb N-glycosylation at the stage of building complex glycans, which takes place within the GA.

Figure 5. Salinomycin and monensin suppress synthesis of complex N-glycan structures of secreted proteins. (A) Comparative analysis of N-glycans from secreted proteins of mock, Sal and Mon treated non-EMT (HMLE-pBp, left panel) and EMT cells (HMLE-Twist, right panel). The glycans were separated into oligomannose, hybrid and complex glycans (shading box colours follow the scheme in (F)). Each area under the peak from chromatograms (Fig. S6) was integrated and its relative amount for each glycan type was summed and plotted (n = 9, 3 technical replicates from each of 3 biological experiments). Total relative amount of sialylated glycans (B) and degree of sialylation by number of sialic acid residues present on each glycan structure (C). (D) Distribution of branched glycan structures organized by number of antennas. (E) Degree of fucosylated glycan structures organized by the number of fucose residues present. (F) Scheme of N-glycan structures organized by glycan types: oligomannose, hybrid and complex. Background colour corresponds to glycan type in A and Figure S5D.

(G) Proposed mechanism of ionophores' selectivity against EMT cells. The process of epithelial-mesenchymal transition (EMT) has significant effects on the protein processing, glycosylation, and secretion within the Golgi apparatus (GA). During EMT, cells undergo a phenotypic transformation characterized by changes in cell adhesion, migration, and invasion. These changes are accompanied by alterations in the GA morphology and its associated functions. Ionophores cause dissipation of the H^+ gradient across the Golgi membrane and affect the GA depending on EMT status and/or at different sites. This in turn leads to disruption of normal protein processing, glycosylation, and secretion. Improperly processed and/or glycosylated proteins accumulate in the ER and the GA inducing ER stress and UPR. On the other hand, abnormal protein trafficking and glycosylation impede normal cell signalling and communication, leading to diminished EMT maintenance, and in non-EMT cells, induction of cholesterol, lipid, and alcohol biosynthesis. One-way ANOVA with post-hoc Tukey's multiple comparison test was used for statistical analysis from n = 3 individual experiments (ns – non significant, ***$p < 0.001$)

Discussion

Salinomycin has been in the spotlight of cancer research ever since its EMT/CSC selective capabilities were revealed (Gupta et al., 2009). While numerous effects of Sal in different cellular models were reported, the mechanism of its selectivity against EMT cells remained elusive. Our work, for the first time, establishes Sal as a Golgi apparatus disturbing agent, positioning it along with established GA inhibitors, monensin and nigericin. The EMT/CSC selectivity of Mon was also recently experimentally confirmed in a prostate cancer model (Vanneste et al., 2019). In our experiments, both Sal and Mon lead to marked morphological perturbations of the GA accompanied by hindered post-translational protein modifications, elevated ER-stress and UPR, diminished secretion and highly altered N-glycosylation of secreted proteins. These changes induce the expression of the ER, the GA, and membrane-related genes, pointing to problems in the secretory pathway.

Differential response of EMT and non-EMT cells to Golgi-disturbing agents

Sal targeted GA in both EMT and non-EMT cells. However, the individual responses were largely different and resulted in differential outcomes in EMT and non-EMT cells. Importantly, the effect of Sal are concentration-dependent and selectivity is achieved at low concentrations (0.2 μM). Our results showed that Sal caused a strong fragmentation of Golgi cisternae in HMLE-Twist (EMT) cells, whereas it had no similar effect in their non-EMT counterparts. However, the GA of EMT cells was on average much more condensed than that of non-EMT cells. Although this may be a specific feature of this particular cell model (HMLE), EMT has been shown to induce the compaction of GA by high levels

of a scaffold protein PAQR11 in EMT-driven lung adenocarcinoma models (Tan et al., 2017). However, systematic evaluation has yet to provide evidence for the universality of this phenomenon.

We also demonstrated that Sal specifically targets the GA and, like Mon and Nig, primarily affects the trans-Golgi compartment. For example, we observed incomplete proteolytic removal of the N-cadherin prodomain in EMT cells after Sal and Mon. Activation of cadherins requires proteolytic removal of their prodomain in the late GA compartments (TGN) by proprotein convertases, most likely furin (Koch et al., 2004; Maret et al., 2010). However, the removal of E-cadherin prodomain in non-EMT cells (HMLE-pBp, HMLE-shGFP or MCF-7), which requires same proprotein convertases, was not inhibited by Sal. On the other hand, BFA, which inhibits vesicle formation between the ER and the GA, also impaired proteolytic cleavage, but only in non-EMT cells and also showed selectivity toward HMLE EMT model cells. It has been shown that compartmentalization of enzymes located at the GA can vary between different cell types, leading to different effects in different cell models (Rosa et al., 1992). Consequently, BFA may not exert the same effect on GA function that Sal does.

In addition, we primarily detected diminished relative amounts of complex N-glycan structures after the treatment with Sal and Mon. All glycosyltransferases that introduce and process components of complex N-glycans (e.g. MGATs – branching, STGALs – sialylation and FUTs – fucosylation) are found within cisternae of the GA, mostly in TGN (Varki et al., 2009). Furthermore, we observed the activation of ER-related UPR, which was already established as the mechanism behind the selectivity towards EMT cells (Feng et al., 2014). The activation of UPR in our experimental setting is likely a downstream effect of inducing the GA-stress through the excessive accumulation of properly folded proteins. It was previously shown that the inhibition of N-glycosylation inside the GA leads to the accumulation of improperly glycosylated proteins within the GA, the diminished secretion of proteins and the induction of the ER-stress related UPR (Xu et al., 2010). In our study, Sal activated PERK and not the IRE1 branch of UPR, positioning it in different cluster of UPR activating compounds together with Mon and BFA, contrary to the cluster containing tunicamycin and thapsigargin (Shinjo et al., 2013).

Potential mechanism of activity/selectivity

Maintenance of acidic compartments of the secretory pathway is crucial for proper protein processing, glycosylation, and sorting, as well as the organelle morphology (Rivinoja et al., 2012; Weisz, 2003). We hypothesize that Sal leads to alkalinization of the GA by an increased release of protons from the organelle in exchange for K^+ ions, similar to the effect of Mon and Nig (Fig. 5G). However, Sal and Mon diversely affect the GA in regard to their EMT status, and/or at different points within this organelle. This, in turn, selectively affected viability of EMT cells, most probably by abrogating their proper maintenance.

It has been previously shown that increased sensitivity of EMT-like cells to Mon is associated with increased uptake of Mon compared to resistant cells (Vanneste et al., 2019). Our results clearly show a pronounced effect of lower concentrations of Sal on protein processing in EMT cells, which was lost at higher concentrations, suggesting more severe effects on the cells and possibly causing the loss of selectivity. However, the data from this study do not rule out selective uptake of Sal as suggested by Vanneste et al. for Mon, possibly due to different cell lines and methods used to assess this issue. For example, in the published study on uptake of Mon, a radiolabelled compound was used to measure uptake, and data were measured at different time points. In contrast, the data in this study were obtained at a single time point and were undetectable after treatment of the cells with a Sal concentration of 0.2 µM, which was important for selectivity. Therefore, further optimisation of the measurements for Sal concentration should be sought in order to draw clear conclusions about the selective uptake of Sal. In addition, it is conceivable that Mon and Sal have different cell penetration abilities, and while brefeldin A has some selectivity, its effect on the function of the GA may not be comparable to that of Sal.

Furthermore, Mon was shown to exert its best ionophoric activity in the cholesterol-rich membranes (trans-Golgi) as compared to the low-cholesterol membranes (cis-Golgi) (Dinter and Berger, 1998; Orci et al., 1981). It was found that the variable lipid/cholesterol environments within organelles regulate traffic of membrane proteins (Lippincott-Schwartz and Phair, 2010). Although critical for the maintenance of normal cellular function, the relationship between cholesterol homeostasis in organelles and EMT is not well understood. Therefore, it remains an open question whether the observed different outcomes between EMT and non-EMT cells are the result of the different degree of alkalinization and/or cholesterol distribution as well as the different GA morphology.

Changes in glycosylation are of major importance for understanding the significance of the EMT during carcinogenesis (Taniguchi and Kizuka, 2015). Interestingly, the effects on N-glycosylation were very similar in EMT and non-EMT cells. Although we only measured the effects on N-glycosylation of secreted proteins, we can assume that the changes in glycan structures also extend to nonsecreted and membrane proteins, as well as to additional glycosylation classes processed within the GA (e.g., O-linked and lipid glycosylation, glucosaminoglycans), which may be the reason for the different sensitivity of EMT and non-EMT cells.

In addition, our study builds on the seminal research that highlighted ER stress as a vulnerability of cancer cells undergoing EMT due to the excessive synthesis and secretion of ECM proteins by EMT cells (Feng et al., 2014). Our analysis of gene expression data after treatment with Sal confirmed the enrichment of ECM-related genes specifically in EMT cells, suggesting a role for the GA in regulating ECM organization and cell adhesion. The GA plays a critical role in coordinating posttranslational

modifications and proteolytic processing of ECM components, which may have far-reaching effects on ECM function (Hellicar et al., 2022). However, the precise impact of the GA on ECM remodelling in cancer has not been fully elucidated, and further studies are needed. Despite the gaps in our knowledge, the consistent findings of an enrichment of ECM-related genes in EMT cells and their response to Sal treatment support the importance of the GA in controlling ECM production and function.

Conclusion

Described observations led us to conclude that EMT cells are sensitive to Golgi-disturbing agents, first, because they are highly dependent on the function of the GA and, second, because significant differences between the structure and function of the GA in epithelial and mesenchymal cells may be the reason for the different outcomes. Our results, most of which were obtained from a specific EMT model, did not reveal explicit targets that clearly prove that the GA is critical for EMT selectivity. Moreover, the ionophores used in this study target multiple aspects of the GA function and are known to have various toxic effects on the whole organism (Boehmerle et al., 2014). Nevertheless, we believe that this work should stimulate further studies focused on elucidating the mechanisms that regulate the function of the GA in EMT and that could lead to therapeutic targeting of individual components. Elucidation of the specific GA -related processes would lead to the development of more precise inhibitors with better efficacy and lower toxicity. For example, a recent study identified two novel regulators of GA -secretion as potential drug targets in lung cancer (Bajaj et al., 2020). Similarly, Eisenberg-Lerner et al. have shown that disruption of GA homeostasis triggers multiple myeloma cell death *in vitro* and *in vivo*, providing a therapeutic strategy for this type of cancer cells, which are highly involved in protein glycosylation and secretion (Eisenberg-Lerner et al., 2020).

Given the strong relationship between the GA architecture and a number of higher-order functions triggered by this organelle, such as cell polarisation, attachment, migration, proliferation, mitosis, differentiation, etc. and its close physical and functional connection with the ER, it is surprising that the GA has remained a largely unexplored target for drug intervention. The finding that EMT cells are sensitive to Golgi-disturbing agents is important not only for the treatment of highly malignant tumours, especially those with a high proportion of EMT cells, but also for uncovering broader implications of the GA in EMT plasticity. Further studies on the regulatory mechanisms controlling the function of the GA in other epithelial and mesenchymal cells will be important.

Methods

Cell culture and reagents

HMLE cells expressing Twist or empty vector (HMLE-Twist and HMLE-pBp) were kindly provided by Dr. Tamer T. Onder, HMLE cells expressing shRNA targeting E-cadherin or GFP (HMLE-shEcad and HMLE-shGFP) and SUM 159 were kindly provided from Dr. Robert A. Weinberg's laboratory. HMLE cells were maintained in a 1:1 mixture of HuMEC Ready Medium (Gibco) and DMEM complemented with 10% FBS, 2 mM L-glutamine, 100 U/mL penicillin, 100 µg/mL streptomycin, 2.5 µg/ml insulin and 0.5 µg/mL hydrocortisone (Sigma-Aldrich). MCF-7 and MDA-MB-231, HepG2 and HCT 116 cell lines were obtained from ATCC, and maintained in DMEM complemented with 10% FBS, 2 mM L-glutamine, 100 U/mL penicillin and 100 µg/mL streptomycin, while SUM 159 cells were grown in Ham's F12 media with 5% FBS, 1 µg/ml hydrocortisone and 5 µg/ml insulin (Sigma-Aldrich). HeLa cells stably expressing the trans-Golgi marker GalT-GFP and H2B-mCherry (Neumann et al., 2010) were kindly provided by Dr. Rainer Pepperkok and maintained at the Advanced Light Microscopy Core Facility (ALMF), EMBL, Heidelberg, Germany. All cells were grown in a humidified atmosphere at 37°C with 5% CO_2, and were tested for mycoplasma contamination on a regular basis. EMT and non-EMT status was regularly checked by probing for EMT markers (CD24/CD44 by FACS and E- and N-cadherin by western blot). Salinomycin (S4526), nigericin (N7143), monensin (46468), paclitaxel (T7402), tunicamycin (T7765), brefeldin A (B6542), bafilomycin A (B1793) and GalNAc(α)-O-bn (B4894) were purchased from Sigma-Aldrich.

Proliferation assays

MTT. Cells were seeded (3000 per well) in standard 96-well microtiter plates and left to attach. Next day, test compounds were added at 10 different concentrations in quadruplicates. The cell growth rate was evaluated after 72 hours of incubation by adding MTT reagent (Sigma-Aldrich). Obtained results for each compound were calculated and normalized to mock-treated cells. Dose-response curves were plotted in GraphPad Prism using non-linear fit.

Flow Cytometry. For mixed culture experiments, cells were seeded in 6-well culture plates at 1:1 ratio (75000 EMT and 75000 non-EMT cells) and left to attach. Next day, media was replaced by media containing vehicle (DMSO) or tested compound. After 72 hours of treatment, cells were detached, washed in blocking solution (2% BSA in PBS) and immunolabeled with anti-CD24 PerCP/Cy5.5 and anti-CD44 FITC primary antibodies (BioLegend, 1:50, 311115 and 1:100, 338803, respectively) for 30 minutes at RT. Cells were then washed twice with PBS and transferred to FACS tubes. 10000 cells were analyzed on a BD FACSCalibur, and percentages of CD24/CD44 specific populations were calculated in FlowJo (TreeStar, Inc.).

Western blot

Cells were collected by trypsinization, pelleted and washed with PBS on ice. Pellets were lysed with RIPA buffer supplemented with complete protease inhibitor (Roche) supplemented with phosphatase inhibitors (NaF and Na_3VO_4, Sigma-Aldrich) and subsequently sonicated using Bioruptor (Diagenode). Total concentration of proteins in cell lysates was measured by Pierce BCA Protein Assay Kit (Thermo Fisher Scientific) according to the recommendations from the manufacturer. 50 µg of protein per sample were loaded on a gel, separated using SDS-PAGE and transferred to PVDF membrane (Carl Roth). After protein transfer, membranes were stained using naphthol blue solution (0.1% naphthol blue in 10% methanol, 2% acetic acid) to visualize transferred proteins that was used to evaluate equal sample loading. Next, membranes were incubated in blocking solution (5% non-fat milk in TBST) for 20 minutes at room temperature. After blocking, membranes were incubated with primary antibodies at 4°C overnight. Primary antibodies used: E-cadherin (1:500, Becton-Dickinson, 610181), N-cadherin (1:500, Becton-Dickinson, 610920), proN-cadherin (1:500, R&D Systems, AF1388), EGFR (1:1000, Cell Signaling Technology, 4267), TFRC (1:500, Thermo Fisher Scientific, 13-6800), eIF2α (1:1000, Cell Signaling Technology, 9722), p-eIF2α (1:1000, Cell Signaling Technologies, 3597), CREB-2 (1:100, SCBT, sc-200). After washing the membranes with TBST, membranes were incubated with complementary HRP conjugated secondary antibody (sheep anti-mouse IgG-HRP, 1:10000, GE Healthcare, NA931; goat anti-rabbit IgG-HRP, 1:5000, Bio-Rad, 1706515; rabbit anti-sheep IgG-HRP, 1:3000, Invitrogen, 61-8620) for 2 hours at room temperature and subsequently washed again with TBST before detection of signal by Western Lightning Plus-ECL reagent (Perkin-Elmer, USA). Emitted signal from membranes was collected and visualized with UVITEC imaging system (Cleaver Scientific Ltd) and final images were prepared in Photoshop CS2 and Illustrator CS2 (Adobe). Uncropped images of the blots shown in Figs 3, 4 and S4 are shown in Fig. S6. To remove N-glycans from proteins, cell lysates were additionally treated with 16 units of PNGase F (New England Biolabs) per µL of lysate complemented with 1% NP-40. De-glycosylation reaction was performed at 37°C for 60 minutes.

Microscopy

Cells were seeded onto poly-L-Lysine treated glass cover slides, left to attach and the next day treated with compounds as indicated. Cellular compartments were stained according to the following protocol: After 24 hours of incubation slides were fixated with 4% PFA in PBS for 10 minutes and then permeabilised with blocking solution (2% BSA, 0.05% Tween-20 in PBS) for another 10 minutes. Slides were then incubated with primary antibody in blocking solution for 30 minutes at room temperature (RT). Primary antibodies used: GM130 (1:500, BD Biosciences, 610822), GIANTIN (1:2000, Abcam, ab24586), ERGIC53 (1:1000, Enzo Life Sciences, ALX-804-602) and β'COP (1:500, rabbit polyclonal anti-β'COP antibody was a kind gift from Dr. Rainer Pepperkok, EMBL Heidelberg).

Slides were then washed and incubated with complementary goat anti-rabbit Alexa Fluor 488, goat anti-mouse Alexa Fluor 568 or goat anti-mouse Alexa Fluor 488 secondary antibody (Thermo Fisher Scientific, A-11034, A-11031 and A-11001, respectively) diluted 1:300 in blocking solution at RT. In the end, slides were extensively washed with blocking solution, and in the last washing step 100 ng/mL of DAPI was used as a counter stain for DNA. Slides were then mounted onto glass slides using Fluoromount antifade reagent (Sigma-Aldrich). Images were collected on a Leica SP8 confocal microscope, processed in ImageJ and prepared for publication in Illustrator CS2 (Adobe). Live-cell imaging of HeLa cells stably expressing the fluorescent markers H2B-mCherry and GalT-GFP for 24 h at a time-lapse of 15 min was performed with automated epifluorescence microscope (IX-81; Olympus Europe) using an in-house modified version of ScanR and an image-based autofocus routine, as described previously (Neumann et al., 2010).

RNA-Seq

Cells were seeded onto 10 cm plates (1.3 million cells per plate) and left to attach overnight. Next day, media was replaced by media containing vehicle (DMSO) or 0.2 µM Sal. Ater 24 hours, total RNA from biological triplicates of HMLE-Twist and HMLE-pBp cells was extracted (12 biological samples in total) with Quick-RNA Miniprep kit (Zymo Research) according to manufacturer protocol. DNase I was used to remove possible DNA contamination. RNA concentration was measured on Qubit 3.0 Fluorometer (Thermo Fisher Scientific) and the quality of RNA was additionally checked with Bioanalyzer 2100 (lowest RIN = 9.7, Agilent). cDNA library was prepared with TrueSeq Stranded mRNA kit (Illumina) from 750 ng of RNA (average cDNA size was ~345bp). Library was sequenced on NextSeq500 (Illumina) using high output flow-cell in paired-end mode (75 + 75 cycles). Raw data yielded over 690 million high-quality reads (Q30 > 75%). Reads were uploaded to BaseSpace Sequence Hub (Illumina) and aligned to human reference genome (hg19) via RNA-Seq Alingment app (STAR alignment, ver 1.1.1). Differential expression of genes after treatment for each cell line and between EMT and non-EMT cell lines was executed via DESeq2 app (ver 1.1.0) in paired mode. The data discussed in this publication have been deposited in NCBI's Gene Expression Omnibus (Edgar et al., 2002) and are accessible through GEO Series accession number (GSE124975).

Gene Ontology and GSEA

GO. For Gene Ontology analysis we used Gene Ontology Enrichment Analysis and Visualization tool (GOrilla, http://cbl-gorilla.cs.technion.ac.il/) by loading single ranked genes from each differential gene expression experiment (genes were ranked according to differential expression from highest to lowest). Additionally, we performed GO analysis of overlapping genes from different experimental

settings with Panther GO algorithm (http://www.geneontology.org/). Venn diagrams were plotted via web tool of Ghent University (http://bioinformatics.psb.ugent.be/webtools/Venn/).

GSEA. For gene set enrichment analysis (GSEA), expression data obtained after treatment with Sal in both EMT and non-EMT cells was analyzed for enrichment of top 100 genes induced by monensin (GSE5258), nigericin and HyT36 Golgi UPR (Serebrenik et al., 2018) (GSE99490), doxorubicin (GSE39042), 4MU-xyloside (GSE117938), brefeldin A (GSE94861), tunicamycin and thapsigargin (GSE24500). In addition, GSEA was performed for genes in gene ontology category Glycosylation downloaded from Molecular signature database (MsigDB). All GSEA analyses were executed with the use of GSEA software downloaded from Broad Institute (MIT)(Subramanian et al., 2005).

Elucidation of additional EMT selective compounds

Raw data from initial compound screen by Gupta et al. (6) was downloaded and analyzed in R. To generate additional compounds with selective properties we performed 3 algorithms, which yielded 32, 54 and 183 compounds combining to total of 227 unique compounds. Algorithms: 1) shGFP BsubvalueA (or B) > of mean of BsubvalueA (or B) AND shEcad ZscoreA (or B) is < mean – 1 s.d. of ZscoreA (or B); 2) shGFP BsubvalueA (or B) > of mean of average (BsubvalueA, BsubvalueB) AND shEcad ZscoreA (or B) is < mean – 1 s.d. of ZscoreA (or B); 3) shGFP BsubvalueA (or B) > of mean- 1 s.d. of BsubvalueA (or B) AND shEcad ZscoreA (or B) is < mean – 2 s.d. of ZscoreA (or B).

RT-PCR

For the analysis of UPR-related splicing of XBP1, 150000 cells were seeded in 6-well plates and left to attach. Next day, media was replaced with media containing vehicle (DMSO) or tested compounds. After 24 hours of treatment, cells were washed with ice-cold PBS and RNA was isolated from cells using TRIzol reagent (Sigma). Reverse transcription and subsequent PCR amplification was done with OneTaq RT-PCR Kit (New England Biolabs). Primers: GAPDH-For (gagtcaacggatttggtcgt), GAPDH-Rev (ttgattttggagggatctcg), XBP1-For (aaacagagtagcagctcagactgc) and XBP1-Rev (tccttctgggtagacctctgggag).

ELISA

Cells were grown in 24-well plates (75000 cells/well) in 1 mL media containing vehicle (DMSO) or compounds. After 24 hours, media above cells was collected and analyzed for the amount of IL-8 secreted. ELISA was performed with Human IL-8 ELISA Ready-SET-Go kit (Affymetrix eBioscience) according to manufacturer's protocol.

Nile Red staining

Cells were seeded onto poly-L-Lysine treated glass cover slides, left to attach and the next day treated with compounds as indicated. Lipid droplets were stained according to the following protocol: After 24 hours of incubation slides were washed with PBS twice and then fixated with 4% PFA in PBS for 15 minutes at RT. After fixation, cells were again washed twice with PBS and then stained with 150 nM Nile Red (Sigma-Aldrich, 72485) in PBS for 15 minutes at RT. Cells were then washed with PBS twice and mounted onto microscopy slides using Fluoromount antifade reagent containing 100 ng/mL DAPI (Sigma-Aldrich). Images were collected on a Leica SP8 confocal microscope, processed in ImageJ and prepared for publication in Illustrator CS2 (Adobe).

Measuring cytosolic calcium

Flow cytometry. 500000 cells in suspension were loaded with 3 µM Fluo-4 AM (Thermo Fisher Scientific, F14201) in DMEM without serum supplemented with 0.02% Pluronic-F127 (Sigma, P2443) for 60 min at 37°C. The cells were then washed in HBSS and left in DMEM without serum for additional 20 minutes at 37°C to allow complete de-esterification of intracellular Fluo-4 AM. Cells were then washed twice with HBSS and, after the last wash a 400 µL of compound in HBSS was added to cells (final concentration as indicated). Green fluorescence of 10000 cells was measured 10 and 30 minutes after the addition of compound on a BD FACSCalibur. The collected data was further analyzed in FlowJo (TreeStar, inc.).

Confocal imaging. 25000 cells were seeded on a 3.5 cm dishes with glass bottom (IBIDI, 81156) and left to attach overnight. On the day of imaging, cells were loaded with Fluo-4 AM as for flow cytometry above. For fluorescence imaging, cells were washed twice with HBSS and 1.2 mL was left over cells for imaging. After desired area with cells was found, cells were imaged every 15 seconds for 10 minutes. 400 µL of 4× concentration of compound in HBSS was added directly to the cells (final concentration indicated) under the microscope before the second image (after ~10 seconds). Images were collected on a Leica SP8 confocal microscope with 40× immersion objective. The Fluo-4 fluorescence intensity of multiple cells was measured in ImageJ and normalized to the same cell from the first image.

Analysis of mitochondrial depolarization

500000 cells in DMEM were treated with salinomycin at indicated concentrations. After 30 minutes of incubation 2.5 µg/mL of JC-1 mitochondrial potential fluorescent probe (eBioscience, EBI-65-0851-38) was added to the cells for additional 30 minutes of incubation (1h total of Sal treatment). Cells were then placed on ice and analyzed on a BD FACSCalibur flow cytometer, and percentages of red and green fluorescent specific populations were calculated in FlowJo (TreeStar, Inc.).

Analysis of the N-Glycome on secreted proteins

Cells were seeded onto 10 cm plates (1 million cells per plate) and left to attach overnight. Next day, media was discarded, cells were washed with PBS 4 times and 9 mL of media (without FBS or supplements) containing vehicle (DMSO) or compound was added to each plate. After 48 hours, plates were placed on ice, media was collected into tubes and residual cells and large debris was pelleted at 2000g. Supernatant was collected and concentrated with Amicon Ultra centrifugal filter devices with 10 kDa cut-off membrane (Merck). Protein concentration was measured by Pierce BCA Protein Assay Kit (Thermo Fisher Scientific) according to the recommendations from the manufacturer. 15 µg of proteins from each sample were denatured with the addition of SDS and by incubation at 65 °C. The excess of SDS was neutralized with Igepal-CA630 (Sigma-Aldrich) and N-glycans were released following the addition of PNGase F (Promega) in PBS. The released N-glycans were labeled with 4-amino-N-(2-diethylaminoethyl) benzamide (Procainamide; ProA). Free label and reducing agent were removed from the samples using hydrophilic interaction liquid chromatography solid-phase extraction (HILIC-SPE). Fluorescently labeled N-glycans were analyzed by HILIC-UPLC-FLR-MS/MS on an Acquity UPLC instrument (Waters) consisting of a quaternary solvent manager, sample manager, and an FLR fluorescence detector set with excitation and emission wavelengths of 310 and 370 nm, respectively. N-glycans were separated on a Waters BEH Glycan chromatography column, 150 × 2.1 mm i.d., 1.7 µm BEH particles, with 100 mM ammonium formate, pH 4.4, as solvent A and ACN as solvent B. The separation method used a gradient of 32-38% solvent A for 16 min and 38%-55% solvent A for next 24 min. Flow rate of 0.56 mL/min was constant during the whole analytical run. Samples were maintained at 10 °C before injection, and the separation temperature was 25 °C. The UPLC was hyphenated to the Bruker compact Q-Tof mass spectrometer (MS), both controlled using HyStar software (Bruker) version 4.1. UPLC was coupled to MS via Ion Booster (Bruker) ion source. Capillary voltage was set to 2250 V with nebulizing gas at pressure of 5.5 Bar. Drying gas was applied to source at a flow rate of 4 L/min and temperature of 300 °C, while vaporizer temperature was set to 300 °C and flow rate of 5 L/min. Nitrogen was used as a source gas, while argon was used as collision gas. Ion energy was set to 5 eV, transfer time was 100 µs. Spectra were recorded in mass range from 50 m/z to 4000 m/z at a rate of 0.5 Hz. For MS acquisition collision energy was set to 4 eV. Fragment spectra were acquired using auto MS/MS mode. HILIC-UPLC-FLR chromatograms were used for quantification, and abundance of each glycan was expressed as percentage of total integrated area. N-glycan compositions and structural features were assigned using GlycoMod (ExPASy) (Cooper et al., 2001) (http://web.expasy.org/glycomod/) and GlycoWorkbench (Ceroni et al., 2008).

Determination and quantification of salinomycin by the LC-MS/MS method

Sample preparation and calibration. HMLE-pBp and HMLE-Twist cell lines were seeded at a concentration of 200 000 cells per well in 6-well plates. The next day, cells were treated in triplicate with Sal (0.2 µM or 5 µM) and incubated for 24 hours. To prepare calibrators, an equivalent number of cells were seeded in five wells without treatment. For cell harvesting, the cell culture medium was removed, and the cells were washed with 2 mL PBS and incubated with 0.33 mL of 0.05% trypsin containing 1 mM ethylenediamine tetraacetate (EDTA, Sigma). After incubation at 37°C for 7 min, cells were collected in 1 mL of complete culture medium in 1.5-mL centrifuge tubes, counted, centrifuged at 250 x G for 5 min, washed with PBS, and centrifuged again to collect the cell pellet. Equal numbers of HMLE-pBp and HMLE-Twist cells were collected for each treatment (0.2 µM and 5 µM Sal) to avoid bias due to lower cell number caused by treatment. Calibration standards were freshly prepared in biological matrix by spiking Sal into the cell pellet samples at final concentrations of 5, 25, 50, 250, and 500 nM for both cell lines individually. 250 nM Sal solution was used as the QC sample. The linearity of the assay was determined from calibration curves obtained by linear regression; peak area was plotted against analyte concentration.

Sample extraction. Sample preparation for mass spectrometry (MS) was performed by a liquid-liquid extraction method modified according to (Li et al., 2010). For extraction from the cell pellet, all samples and calibrants were homogenized for 15 min by vortexing and sonication in 200 µL of PBS. Then, 600 µL of methanol:water (90:10) mixture was added to precipitate the proteins. The mixture was again shaken and sonicated for 15 minutes and then shaken at room temperature for 2 hours to extract the compound of interest (Sal). The samples were centrifuged at maximum speed for 10 minutes, and the supernatant containing the organic phase was transferred to an autosampler vial for analysis MS. The clear solution of the sample or calibrant was injected in a volume of 5 µl onto the LC column.

LC-MS/MS conditions. LC–MS/MS analysis was carried out using an Agilent Technologies 1200 series HPLC system equipped with an binary pump, a vacuum membrane degasser, an automated autosampler and injector interfaced with 6420 triple quadrupole mass spectrometer with electrospray ionization source (ESI) (Agilent Technologies Inc., Palo Alto, CA, USA). The separation was performed on Kinetex C18 column (75 x 4.6 mm, 2.6 µm paricle size) (Phenomenex, Torrance, USA). Solvents for the analysis were 0.1% formic acid (FA) in water (solvent A) and methanol (solvent B). The gradient was applied as follows: 0 min 30% A, 0-12 min 30%-0% A, 12-15 min 0% A, 15.1-20 min 30% A. Flow rate was 0.3 mL/min Retention time of Sal was 15.7 min. The electrospray ionization source was operated in a positive mode and samples were detected in the multiple reaction monitoring (MRM) mode with a dwell time of 200 ms per MRM transition. The desolvation gas temperature was 300 ^{o}C with flow rate of 8.0 L/min. The capillary voltage was 3.5 kV. The collision gas was nitrogen. The MRM transitions of precursor to product ion pairs were m/z 773-531

(qualification transition) and 773-431 (quantification transition). Fragmentor voltage for salinomycin was 135 V and collision energy was set at 40 V. All data acquisition and processing was performed using Agilent MassHunter software.

Statistics

All graphics with error bars are presented as mean ± s.d. except Fig. S3D where mean ± s.e.m. was plotted. To determine statistical significance between samples, one-way ANOVA with Dunnett's (Fig 1A, Fig 1SD, Fig. 3C and D, Fig. S3B) or Tukey's (Fig. 6 and Tables S2 and S3) multiple comparison post-hoc test and two-way ANOVA with Bonferroni's multiple comparisons test was used (Fig. 5B). Statistical calculations were performed in GraphPad Prism and generation of graphics in Excel, R Studio, and Adobe Illustrator CS2 (NS – non-significant; * - $p < 0.05$, ** - $p < 0.01$ and *** - $p < 0.001$).

References

Antoszczak, M. (2019). A medicinal chemistry perspective on salinomycin as a potent anticancer and anti-CSCs agent. *Eur. J. Med. Chem.* **164**, 366–377.

Bajaj, R., Kundu, S. T., Grzeskowiak, C. L., Fradette, J. J., Scott, K. L., Creighton, C. J. and Gibbons, D. L. (2020). IMPAD1 and KDELR2 drive invasion and metastasis by enhancing Golgi-mediated secretion. *Oncogene* **39**, 5979–5994.

Boehmerle, W., Muenzfeld, H., Springer, A., Huehnchen, P. and Endres, M. (2014). Specific targeting of neurotoxic side effects and pharmacological profile of the novel cancer stem cell drug salinomycin in mice. *J. Mol. Med.* **92**, 889–900.

Ceroni, A., Maass, K., Geyer, H., Geyer, R., Dell, A. and Haslam, S. M. (2008). GlycoWorkbench: A tool for the computer-assisted annotation of mass spectra of glycans. *J. Proteome Res.* **7**, 1650–1659.

Cooper, C. A., Gasteiger, E. and Packer, N. H. (2001). GlycoMod - A software tool for determining glycosylation compositions from mass spectrometric data. *Proteomics* **1**, 340–349.

Dewangan, J., Srivastava, S. and Rath, S. K. (2017). Salinomycin: A new paradigm in cancer therapy. *Tumor Biol.* **39**,.

Diaz, G., Melis, M., Batetta, B., Angius, F. and Falchi, A. M. (2008). Hydrophobic characterization of intracellular lipids in situ by Nile Red red/yellow emission ratio. *Micron* **39**, 819–824.

Dinter, A. and Berger, E. G. (1998). Golgi-disturbing agents. *Histochem Cell Biol* **109**, 571–590.

Edgar, R., Domrachev, M. and Lash, A. E. (2002). Gene Expression Omnibus: NCBI gene expression and hybridization array data repository. *Nucleic Acids Res.* **30**, 207–10.

Eisenberg-Lerner, A., Benyair, R., Hizkiahou, N., Nudel, N., Maor, R., Kramer, M. P., Shmueli, M. D., Zigdon, I., Cherniavsky Lev, M., Ulman, A., et al. (2020). Golgi organization is regulated by proteasomal degradation. *Nat. Commun.* **11**,.

Feng, Y. X., Sokol, E. S., Del Vecchio, C. A., Sanduja, S., Claessen, J. H. L., Proia, T. A., Jin, D. X., Reinhardt, F., Ploegh, H. L., Wang, Q., et al. (2014). Epithelial-to-mesenchymal transition activates PERK-eIF2α and sensitizes cells to endoplasmic reticulum stress. *Cancer Discov.* **4**, 702–715.

Geng, F., Zhu, W., Anderson, R. A., Leber, B. and Andrews, D. W. (2012). Multiple post-translational modifications regulate E-cadherin transport during apoptosis. *J. Cell Sci.* **125**, 2615–2625.

Gupta, P. B., Onder, T. T., Jiang, G., Tao, K., Kuperwasser, C., Weinberg, R. A. and Lander, E. S. (2009). Identification of Selective Inhibitors of Cancer Stem Cells by High-Throughput Screening. *Cell* **138**, 645–659.

Hellicar, J., Stevenson, N. L., Stephens, D. J. and Lowe, M. (2022). Supply chain logistics - the role of the Golgi complex in extracellular matrix production and maintenance. *J. Cell Sci.* **135**,.

Huang, X., Borgström, B., Stegmayr, J., Abassi, Y., Kruszyk, M., Leffler, H., Persson, L., Albinsson, S., Massoumi, R., Scheblykin, I. G., et al. (2018). The Molecular Basis for Inhibition of Stemlike Cancer Cells by Salinomycin. *ACS Cent. Sci.* **4**, 760–767.

Huczynski, A. (2012). Salinomycin - A New Cancer Drug Candidate. *Chem. Biol. Drug Des.* **79**, 235–238.

Kalluri, R. and Weinberg, R. a (2009). Review series The basics of epithelial-mesenchymal transition. *J. Clin. Invest.* **119**, 1420–1428.

Kaushik, V., Yakisich, J. S., Kumar, A., Azad, N. and Iyer, A. K. V. (2018). Ionophores: Potential use as anticancer drugs and chemosensitizers. *Cancers (Basel).* **10**, 1–21.

Koch, A. W., Farooq, A., Shan, W., Zeng, L., Colman, D. R. and Zhou, M. M. (2004). Structure of the neural (N-) cadherin prodomain reveals a cadherin extracellular domain-like fold without adhesive characteristics. *Structure* **12**, 793–805.

Lebeau, P. F., Platko, K., Byun, J. H. and Austin, R. C. (2021). Calcium as a reliable marker for the quantitative assessment of endoplasmic reticulum stress in live cells. *J. Biol. Chem.* **296**, 100779.

Lee, L. Y., Thaysen-andersen, M., Baker, M. S., Packer, N. H., Hancock, W. S. and Fanayan, S. (2014). Comprehensive N - Glycome Profiling of Cultured Human Epithelial Breast Cells Identi fi es Unique Secretome N - Glycosylation Signatures Enabling Tumorigenic Subtype Classi fi cation. *J. Proteome Res.* **13**, 4783–4795.

Li, Y., Fang, J., Wu, S., Ma, K., Li, H., Yan, X. and Dong, F. (2010). Identification and quantification of salinomycin in intoxicated human plasma by liquid chromatography-electrospray tandem mass spectrometry. *Anal. Bioanal. Chem.* **398**, 955–961.

Lippincott-Schwartz, J. and Phair, R. D. (2010). Lipids and Cholesterol as Regulators of Traffic in the Endomembrane System. *Annu Rev Biophys.* **39**, 559–578.

Low-Marchelli, J. M., Ardi, V. C., Vizcarra, E. A., van Rooijen, N., Quigley, J. P. and Yang, J. (2013).

Twist1 Induces CCL2 and Recruits Macrophages to Promote Angiogenesis. *Cancer Res.* **73**, 662–671.

Lu, D., Choi, M. Y., Yu, J., Castro, J. E., Kipps, T. J. and Carson, D. A. (2011). Salinomycin inhibits Wnt signaling and selectively induces apoptosis in chronic lymphocytic leukemia cells. *Proc. Natl. Acad. Sci.* **108**, 13253–13257.

Mai, T. T., Hamaï, A., Hienzsch, A., Cañeque, T., Müller, S., Wicinski, J., Cabaud, O., Leroy, C., David, A., Acevedo, V., et al. (2017). Salinomycin kills cancer stem cells by sequestering iron in lysosomes. *Nat. Chem.* **9**, 1025–1033.

Managò, A., Leanza, L., Carraretto, L., Sassi, N., Grancara, S., Quintana-Cabrera, R., Trimarco, V., Toninello, A., Scorrano, L., Trentin, L., et al. (2015). Early effects of the antineoplastic agent salinomycin on mitochondrial function. *Cell Death Dis.* **6**, e1930.

Mani, S. a., Guo, W., Liao, M. J., Eaton, E. N., Ayyanan, A., Zhou, A. Y., Brooks, M., Reinhard, F., Zhang, C. C., Shipitsin, M., et al. (2008). The Epithelial-Mesenchymal Transition Generates Cells with Properties of Stem Cells. *Cell* **133**, 704–715.

Maret, D., Gruzglin, E., Seyed Sadr, M., Siu, V., Shan, W., Koch, A. W., Seidah, N. G., Del Maestro, R. F. and Colman, D. R. (2010). Surface Expression of Precursor N-cadherin Promotes Tumor Cell Invasion. *Neoplasia* **12**, 1066-IN38.

Miyata, S., Mizuno, T., Koyama, Y., Katayama, T. and Tohyama, M. (2013). The Endoplasmic Reticulum-Resident Chaperone Heat Shock Protein 47 Protects the Golgi Apparatus from the Effects of O-Glycosylation Inhibition. *PLoS One* **8**, e69732.

Morré, D. J. and Mollenhauer, H. H. (2009). *The Golgi apparatus: The first 100 years*. (ed. Morré, D. J.) and Mollenhauer, H. H.) New York, NY: Springer New York.

Neumann, B., Walter, T., Hériché, J. K., Bulkescher, J., Erfle, H., Conrad, C., Rogers, P., Poser, I., Held, M., Liebel, U., et al. (2010). Phenotypic profiling of the human genome by time-lapse microscopy reveals cell division genes. *Nat. 2010 4647289* **464**, 721–727.

Nieto, M. A. and Cano, A. (2012). The epithelial-mesenchymal transition under control: Global programs to regulate epithelial plasticity. *Semin. Cancer Biol.* **22**, 361–368.

Nimmakayala, R. K., Batra, S. K. and Ponnusamy, M. P. (2019). Unraveling the journey of cancer stem cells from origin to metastasis. *Biochim. Biophys. Acta - Rev. Cancer* **1871**, 50–63.

Orci, L., Montesano, R., Meda, P., Malaisse-Lagae, F., Brown, D., Perrelet, A. and Vassalli, P. (1981). Heterogeneous distribution of filipin-cholesterol complexes across the cisternae of the Golgi apparatus. *Proc. Natl. Acad. Sci. U. S. A.* **78**, 293–297.

Pattabiraman, D. R. and Weinberg, R. A. (2014). Tackling the cancer stem cells — what challenges do they pose? *Nat. Rev. Drug Discov.* **13**, 497–512.

Rivinoja, A., Pujol, F. M., Hassinen, A. and Kellokumpu, S. (2012). Golgi pH, its regulation and roles

in human disease. *Ann. Med.* **44**, 542–554.

Rosa, P., Mantovani, S., Rosboch, R. and Huttner, W. B. (1992). Monensin and brefeldin A differentially affect the phosphorylation and sulfation of secretory proteins. *J. Biol. Chem.* **267**, 12227–12232.

Sampaio, J. L., Gerl, M. J., Klose, C., Ejsing, C. S., Beug, H., Simons, K. and Shevchenko, A. (2011). Membrane lipidome of an epithelial cell line. *Proc. Natl. Acad. Sci. U. S. A.* **108**, 1903–1907.

Serebrenik, Y. V., Hellerschmied, D., Toure, M., López-Giráldez, F., Brookner, D. and Crews, C. M. (2018). Targeted protein unfolding uncovers a Golgi-specific transcriptional stress response. *Mol. Biol. Cell* **29**, 1284–1298.

Shi, A., Tao, Z., Li, H., Wang, Y. and Zhao, J. (2015). Cancer stem cells targeting agents – a review. *Eur. Rev. Med. Pharmacol. Sci.* **19**, 4064–4067.

Shibue, T. and Weinberg, R. A. (2017). EMT, CSCs, and drug resistance: The mechanistic link and clinical implications. *Nat. Rev. Clin. Oncol.* **14**, 611–629.

Shinjo, S., Mizotani, Y., Tashiro, E. and Imoto, M. (2013). Comparative analysis of the expression patterns of UPR-target genes caused by upr-inducing compounds. *Biosci. Biotechnol. Biochem.* **77**, 729–735.

Smirle, J., Au, C. E., Jain, M., Dejgaard, K., Nilsson, T. and Bergeron, J. (2013). Cell biology of the endoplasmic reticulum and the Golgi apparatus through proteomics. *Cold Spring Harb. Perspect. Biol.* **5**, a015073.

Subramanian, A., Tamayo, P., Mootha, V. K., Mukherjee, S., Ebert, B. L., Gillette, M. A., Paulovich, A., Pomeroy, S. L., Golub, T. R., Lander, E. S., et al. (2005). Gene set enrichment analysis: A knowledge-based approach for interpreting genome-wide expression profiles. *Proc Natl Acad Sci U S A* **102**, 15545–15550.

Tan, X., Banerjee, P., Guo, H. F., Ireland, S., Pankova, D., Ahn, Y. H., Nikolaidis, I. M., Liu, X., Zhao, Y., Xue, Y., et al. (2017). Epithelial-to-mesenchymal transition drives a pro-metastatic Golgi compaction process through scaffolding protein PAQR11. *J. Clin. Invest.* **127**, 117–131.

Taniguchi, N. and Kizuka, Y. (2015). *Glycans and cancer: Role of N-Glycans in cancer biomarker, progression and metastasis, and therapeutics*. 1st ed. Elsevier Inc.

Tseng, C. N., Hong, Y. R., Chang, H. W., Yu, T. J., Hung, T. W., Hou, M. F., Yuan, S. S. F., Cho, C. L., Liu, C. T., Chiu, C. C., et al. (2014). Brefeldin A Reduces Anchorage-Independent Survival, Cancer Stem Cell Potential and Migration of MDA-MB-231 Human Breast Cancer Cells. *Mol. 2014, Vol. 19, Pages 17464-17477* **19**, 17464–17477.

Vanneste, M., Huang, Q., Li, M., Moose, D., Zhao, L., Stamnes, M. A., Schultz, M., Wu, M. and Henry, M. D. (2019). High content screening identifies monensin as an EMT-selective cytotoxic compound. *Sci. Rep.* **9**, 1–15.

Varki, A., Cummings, R. D., Esko, J. D., Freeze, H. H., Stanley, P., Bertozzi, C. R., Hart, G. W. and Etzler, M. E. (2009). *Essentials of Glycobiology*. Cold Spring Harbor Laboratory Press.

Wang, H., Zhang, H., Zhu, Y., Wu, Z., Cui, C. and Cai, F. (2021). Anticancer Mechanisms of Salinomycin in Breast Cancer and Its Clinical Applications. *Front. Oncol.* **11**, 2748.

Weisz, O. A. (2003). Organelle acidification and disease. *Traffic* **4**, 57–64.

Xipell, E., Aragón, T., Martínez-Velez, N., Vera, B., Idoate, M. A., Martínez-Irujo, J. J., Garzón, A. G., Gonzalez-Huarriz, M., Acanda, A. M., Jones, C., et al. (2016). Endoplasmic reticulum stress-inducing drugs sensitize glioma cells to temozolomide through downregulation of MGMT, MPG, and Rad51. *Neuro. Oncol.* now022.

Xu, Y. X., Liu, L., Caffaro, C. E. and Hirschberg, C. B. (2010). Inhibition of Golgi apparatus glycosylation causes endoplasmic reticulum stress and decreased protein synthesis. *J. Biol. Chem.* **285**, 24600–24608.

Yoon, M. J., Kang, Y. J., Kim, I. Y., Kim, E. H., Lee, J. A., Lim, J. H., Kwon, T. K. and Choi, K. S. (2013). Monensin, a polyether ionophore antibiotic, overcomes TRAIL resistance in glioma cells via endoplasmic reticulum stress, DR5 upregulation and c-FLIP downregulation. *Carcinogenesis* **34**, 1918–1928.

Zhao, W., Prijic, S., Urban, B. C., Tisza, M. J., Zuo, Y., Li, L., Tan, Z., Chen, X., Mani, S. A. and Chang, J. T. (2016). Candidate antimetastasis drugs suppress the metastatic capacity of breast cancer cells by reducing membrane fluidity. *Cancer Res.* **76**, 2037–2049.

Acknowledgments

The authors thank Dr. Robert A. Weinberg and Dr. Tamer T. Onder for providing us with HMLE and SUM 159 cell lines. We thank Dr. Rainer Pepperkok and his laboratory for help, expertise and shared reagents regarding microscopy of cellular compartments. Ana-Matea Mikecin Dražić was seconded to the Advanced Light Microscopy Core Facility (ALMF), EMBL, Heidelberg, under WP2 of the FP7-REGPOT-2012-2013-1 InnoMol project. Support from the ALMF Core Facility at EMBL-Heidelberg is acknowledged. We are also thankful to Dr. Siniša Volarević and his laboratory for UPR reagents, Dr. Oliver Vugrek and Filip Rokić for help with RNA-Seq experiment, Lucija Horvat for assistance with confocal microscopy, Dr. Lidija Brkljačić and Dr. Ivanka Jerić for performing the LC-MS/MS analysis of salinomycin and Dr. Fran Supek for critical reading of the manuscript.

Statements and Declarations

Funding

This work was financed by Croatian Science Foundation project (number IP-2013-5660 “MultiCaST”) to MK. The work was also supported by the FP7-REGPOT-2012-2013-1 project (grant agreement

number 316289 – InnoMol) and by the European Structural and Investment Funds IRI (grant KK.01.2.1.01.0003) to GL.

Conflict of interest

GL is the owner of GENOS. The authors declare no other competing interests.

Author Contributions

Marko Marjanović, Ana-Matea Mikecin Dražić and Marijeta Kralj contributed to the study conception and design. Experimental work, analysis of the data, visualization of the data, review and editing of the manuscript were performed by Marko Marjanović, Ana-Matea Mikecin Dražić, Marija Mioč, Mladen Paradžik, Filip Kliček, Mislav Novokmet. The first draft of the manuscript was written by Marko Marjanović and all authors commented on previous versions of the manuscript. All authors read and approved the final manuscript.

Data availability

The datasets generated during the current study are available in the NCBI's Gene Expression Omnibus and are accessible through GEO Series accession number (GSE124975), or are included in this published article and its supplementary information files.

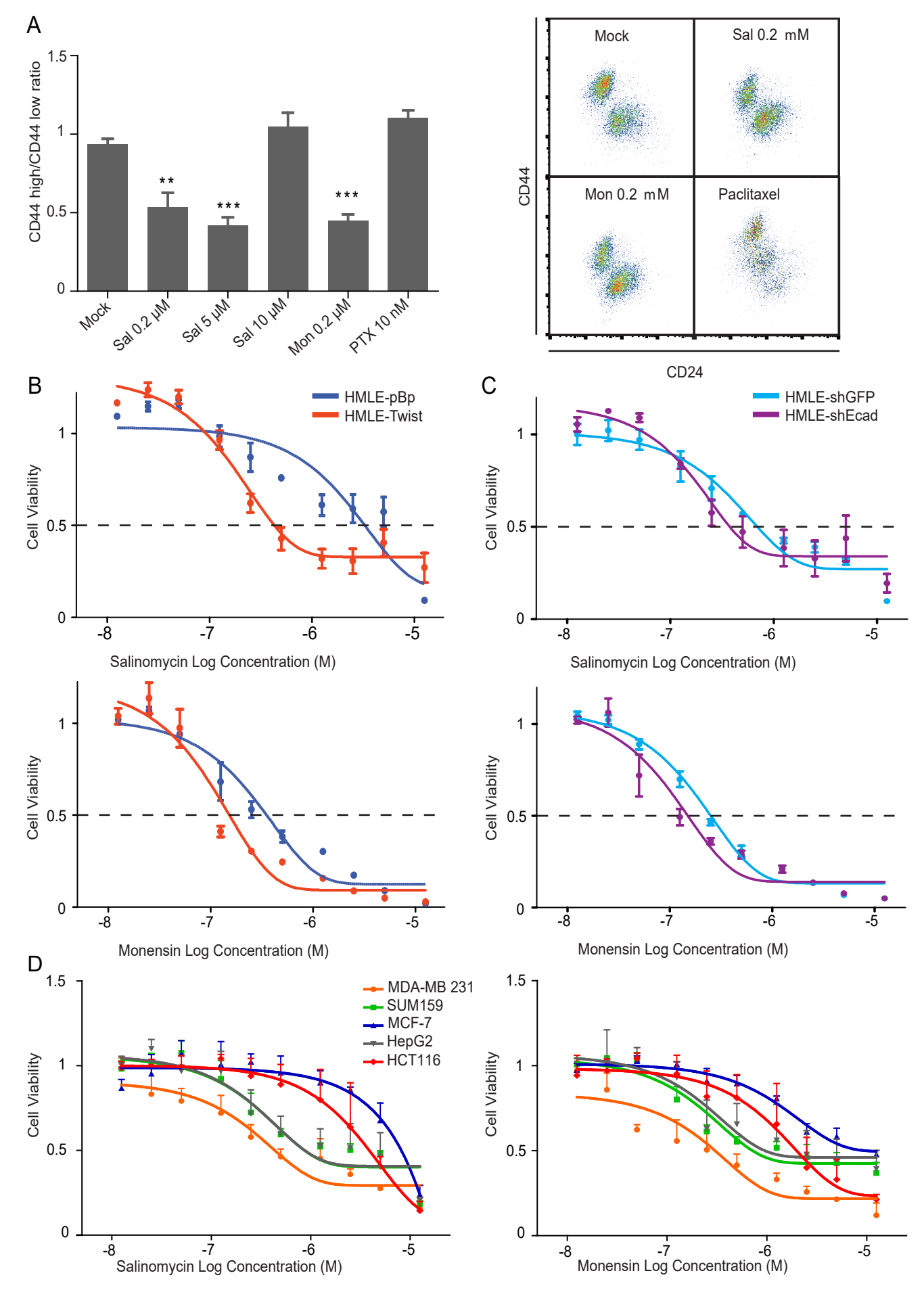
A
CD44 high/CD44 low ratio
1.5
1
0.5
0
**
***
***
Mock
Sal 0.2 μM
Sal 5 μM
Sal 10 μM
Mon 0.2 μM
PTX 10 nM
Mock
Sal 0.2 mM
Mon 0.2 mM
Paclitaxel
CD44
CD24
B
HMLE-pBp
HMLE-Twist
Cell Viability
Salinomycin Log Concentration (M)
C
HMLE-shGFP
HMLE-shEcad
Cell Viability
Salinomycin Log Concentration (M)
Cell Viability
Monensin Log Concentration (M)
Cell Viability
Monensin Log Concentration (M)
D
MDA-MB 231
SUM159
MCF-7
HepG2
HCT116
Cell Viability
Salinomycin Log Concentration (M)
Cell Viability
Monensin Log Concentration (M)

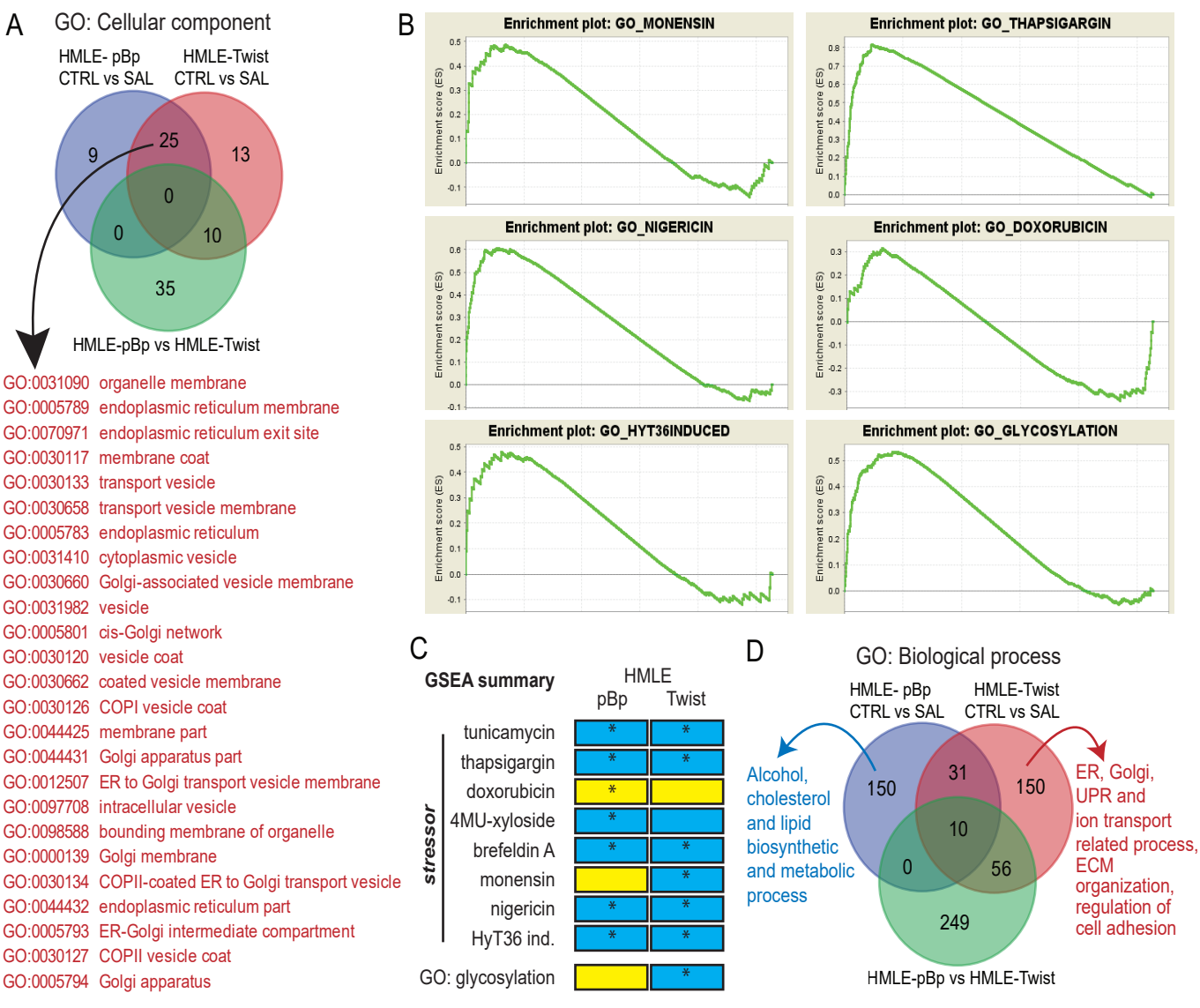
A
GO: Cellular component
HMLE- pBp CTRL vs SAL
HMLE-Twist CTRL vs SAL
9
25
13
0
0
10
35
HMLE-pBp vs HMLE-Twist
GO:0031090 organelle membrane
GO:0005789 endoplasmic reticulum membrane
GO:0070971 endoplasmic reticulum exit site
GO:0030117 membrane coat
GO:0030133 transport vesicle
GO:0030658 transport vesicle membrane
GO:0005783 endoplasmic reticulum
GO:0031410 cytoplasmic vesicle
GO:0030660 Golgi-associated vesicle membrane
GO:0031982 vesicle
GO:0005801 cis-Golgi network
GO:0030120 vesicle coat
GO:0030662 coated vesicle membrane
GO:0030126 COPI vesicle coat
GO:0044425 membrane part
GO:0044431 Golgi apparatus part
GO:0012507 ER to Golgi transport vesicle membrane
GO:0097708 intracellular vesicle
GO:0098588 bounding membrane of organelle
GO:0000139 Golgi membrane
GO:0030134 COPII-coated ER to Golgi transport vesicle
GO:0044432 endoplasmic reticulum part
GO:0005793 ER-Golgi intermediate compartment
GO:0030127 COPII vesicle coat
GO:0005794 Golgi apparatus
B
Enrichment plot: GO_MONENSIN
Enrichment plot: GO_THAPSIGARGIN
Enrichment plot: GO_NIGERICIN
Enrichment plot: GO_DOXORUBICIN
Enrichment plot: GO_HYT36INDUCED
Enrichment plot: GO_GLYCOSYLATION
Enrichment score (ES)
C
GSEA summary
HMLE
pBp
Twist
stressor
tunicamycin
thapsigargin
doxorubicin
4MU-xyloside
brefeldin A
monensin
nigericin
HyT36 ind.
GO: glycosylation
D
GO: Biological process
HMLE- pBp CTRL vs SAL
HMLE-Twist CTRL vs SAL
150
31
150
10
0
56
249
HMLE-pBp vs HMLE-Twist
Alcohol, cholesterol and lipid biosynthetic and metabolic process
ER, Golgi, UPR and ion transport related process, ECM organization, regulation of cell adhesion

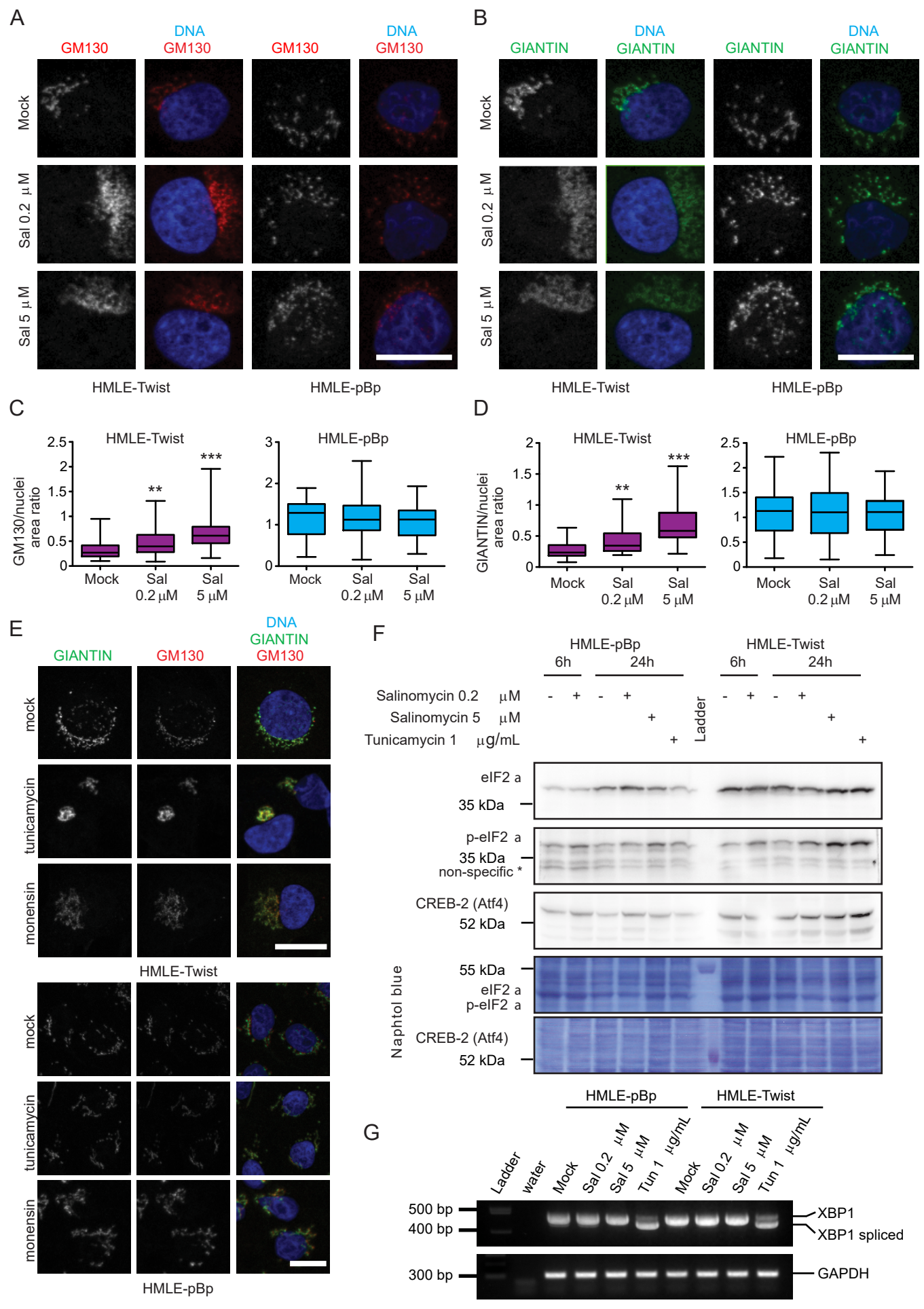
A
GM130
DNA GM130
GM130
DNA GM130
Mock
Sal 0.2 μM
Sal 5 μM
HMLE-Twist
HMLE-pBp
B
GIANTIN
DNA GIANTIN
GIANTIN
DNA GIANTIN
Mock
Sal 0.2 μM
Sal 5 μM
HMLE-Twist
HMLE-pBp
C
HMLE-Twist
HMLE-pBp
GM130/nuclei area ratio
Mock
Sal 0.2 μM
Sal 5 μM
D
HMLE-Twist
HMLE-pBp
GIANTIN/nuclei area ratio
Mock
Sal 0.2 μM
Sal 5 μM
E
GIANTIN
GM130
DNA GIANTIN GM130
mock
tunicamycin
monensin
HMLE-Twist
HMLE-pBp
F
HMLE-pBp
HMLE-Twist
6h
24h
Salinomycin 0.2 μM
Salinomycin 5 μM
Tunicamycin 1 μg/mL
Ladder
eIF2 a
35 kDa
p-eIF2 a
35 kDa
non-specific *
CREB-2 (Atf4)
52 kDa
Naphtol blue
55 kDa
eIF2 a
p-eIF2 a
CREB-2 (Atf4)
52 kDa
G
HMLE-pBp
HMLE-Twist
Ladder
water
Mock
Sal 0.2 μM
Sal 5 μM
Tun 1 μg/mL
500 bp
400 bp
XBP1
XBP1 spliced
300 bp
GAPDH

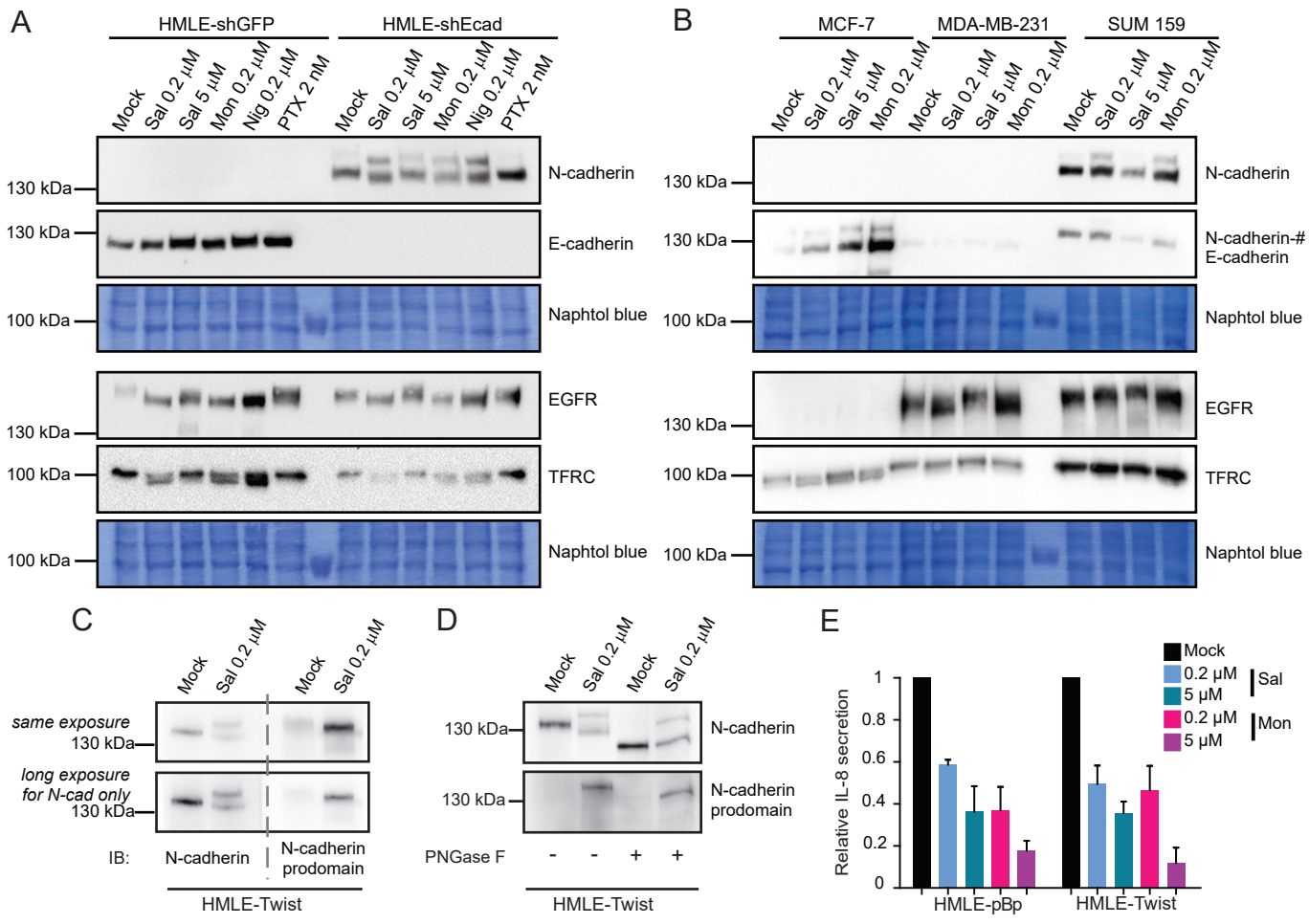
A
HMLE-shGFP
HMLE-shEcad
Mock
Sal 0.2 μM
Sal 5 μM
Mon 0.2 μM
Nig 0.2 μM
PTX 2 nM
130 kDa
N-cadherin
E-cadherin
100 kDa
Naphtol blue
EGFR
TFRC
B
MCF-7
MDA-MB-231
SUM 159
N-cadherin-#
E-cadherin
C
same exposure
long exposure
for N-cad only
IB:
N-cadherin
N-cadherin
prodomain
HMLE-Twist
D
PNGase F
E
Relative IL-8 secretion
Mock
0.2 μM
5 μM
Sal
Mon
HMLE-pBp
HMLE-Twist

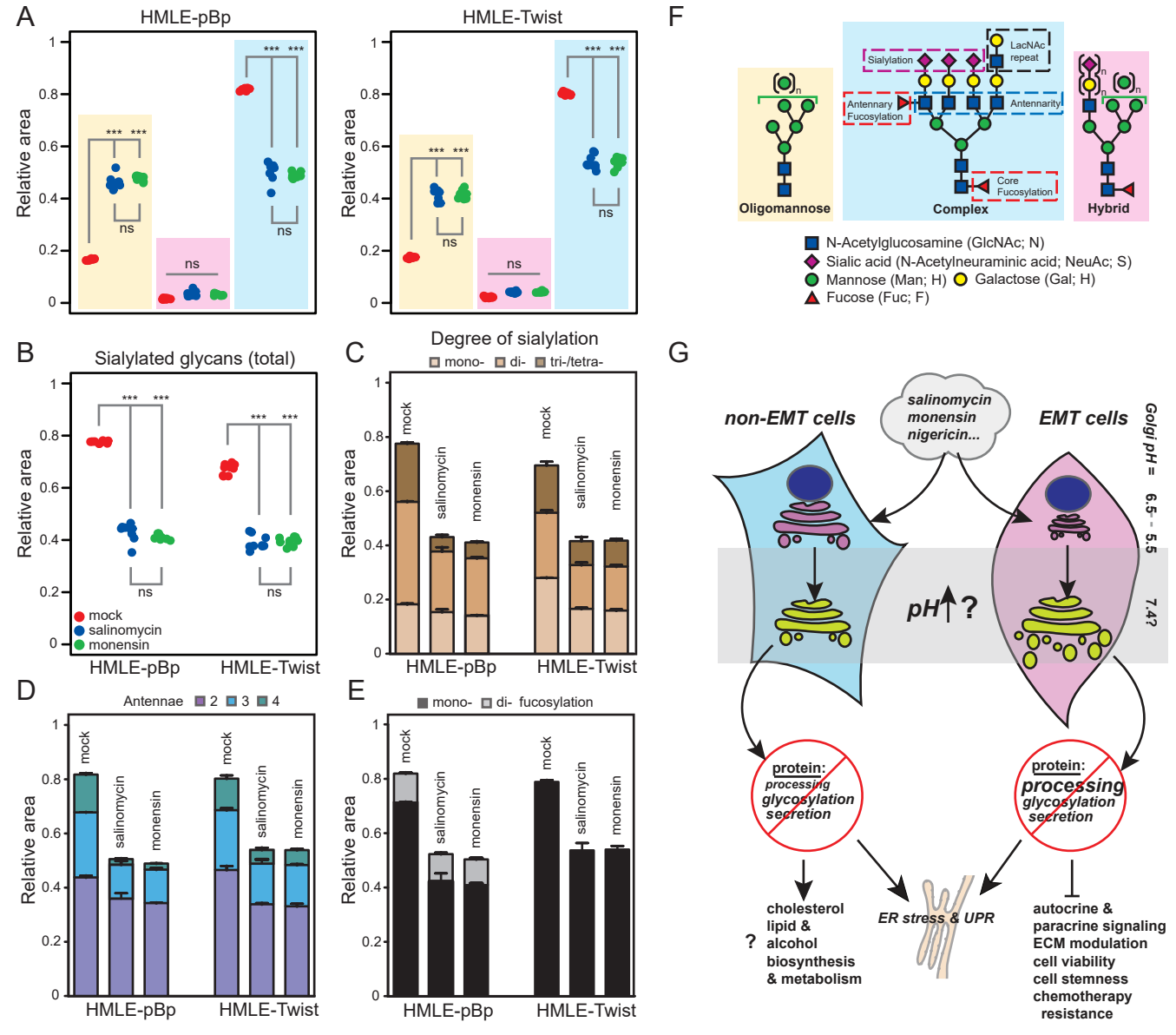
A
HMLE-pBp
HMLE-Twist
Relative area
***
ns
B
Sialylated glycans (total)
mock
salinomycin
monensin
HMLE-pBp
HMLE-Twist
C
Degree of sialylation
mono-
di-
tri-/tetra-
D
Antennae 2 3 4
E
mono- di- fucosylation
F
Sialylation
LacNAc repeat
Antennary Fucosylation
Antennarity
Core Fucosylation
Oligomannose
Complex
Hybrid
N-Acetylglucosamine (GlcNAc; N)
Sialic acid (N-Acetylneuraminic acid; NeuAc; S)
Mannose (Man; H)
Galactose (Gal; H)
Fucose (Fuc; F)
G
non-EMT cells
salinomycin
monensin
nigericin...
EMT cells
Golgi pH =
6.5 - 5.5
7.4?
pH↑?
protein:
processing
glycosylation
secretion
cholesterol
lipid &
alcohol
biosynthesis
& metabolism
ER stress & UPR
autocrine &
paracrine signaling
ECM modulation
cell viability
cell stemness
chemotherapy
resistance

Supplementary Information for

Salinomycin disturbs Golgi apparatus function and specifically affects cells in epithelial-to-mesenchymal transition

Marko Marjanović[a,c,d], Ana-Matea Mikecin Dražić[a,c], Marija Mioč[a, e], Mladen Paradžik[a,f,], Filip Kliček[b], Mislav Novokmet[b], Gordan Lauc[b] and Marijeta Kralj[a,g,*]

[a] Division of Molecular Medicine, Ruđer Bošković Institute, Bijenička c. 54, 10000 Zagreb, Croatia
[b] GENOS, Glycoscience Research Laboratory, Borongajska c. 83, 10000 Zagreb, Croatia
[c] These authors contributed equally
[d] ORCID: 0000-0001-9850-0561

[e] ORCID: 0000-0001-5290-6945

[f] ORCID: 0000-0003-1025-5595

[g] ORCID: 0000-0002-7165-2722

*Corresponding author: marijeta.kralj@irb.hr

This PDF file includes:

Other supplementary materials for this manuscript include the following:

Files S1 to S3 as separate excel files.

Movies 1 and 2 as separate .mp4 files

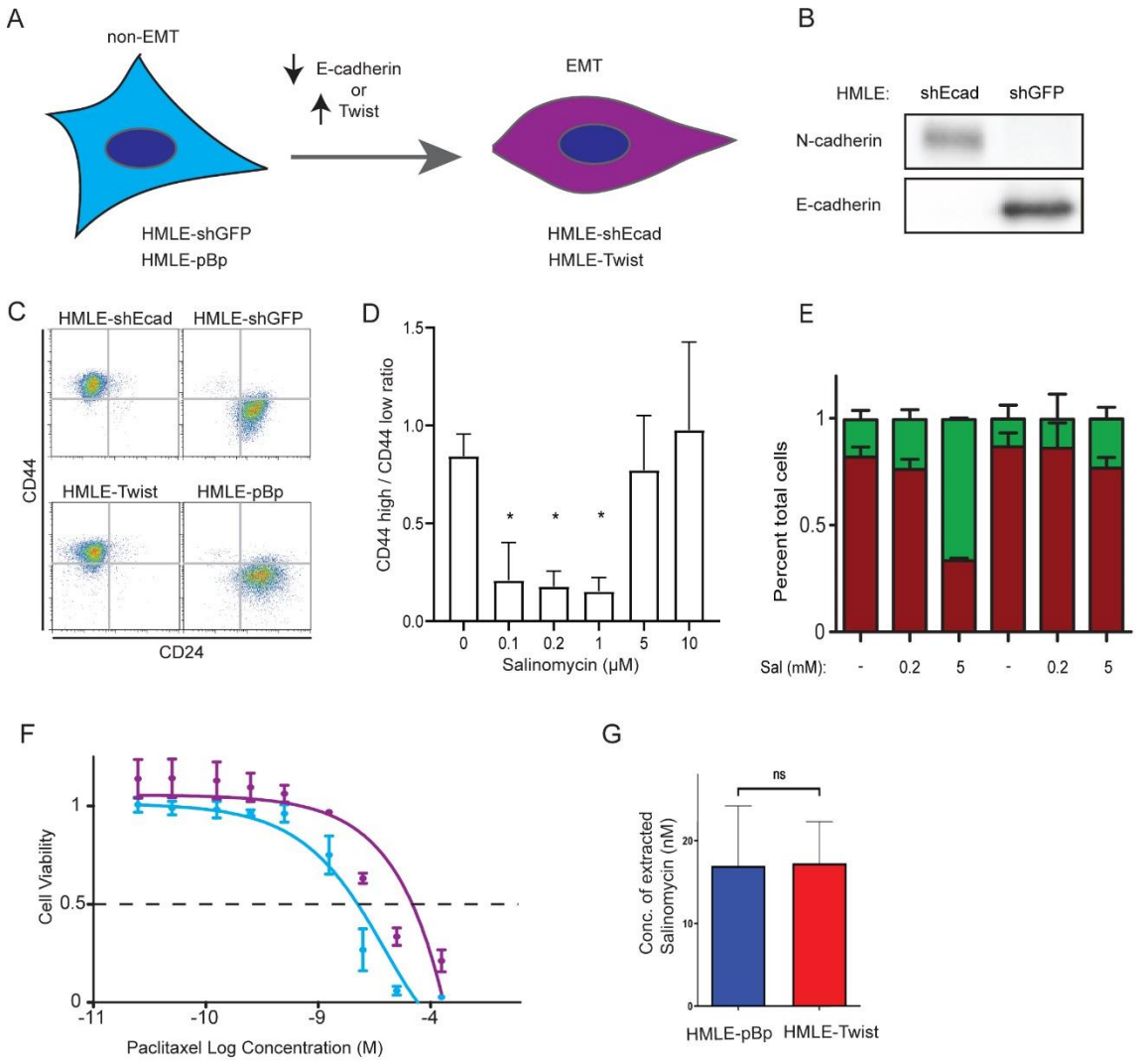

Figure S1. Salinomycin is selective towards EMT cells.
(A) EMT model used in the study.
(B) Western blot analysis of N- and E-cadherin protein expression (EMT and non-EMT marker, respectively) in HMLE-shEcad and HMLE-shGFP cells.
(C) Representative CD24/CD44 flow cytometry profiles of HMLE-shEcad and HMLE-shGFP, HMLE-Twist and HMLE-pBp (EMT and non-EMT cell pairs).
(D) HMLE-shEcad and HMLE-shGFP were seeded on day 0 at 1:1 ratio and then treated with salinomycin (Sal) at increasing concentrations. Ratio of $CD44^{high}/CD44^{low}$ (EMT/non-EMT) cells after 3 days of treatment of mixed culture is shown. Data are presented as mean ± s.d., n = 3 from duplicates.
(E) High concentration of Sal depolarizes mitochondria of non-EMT cells. Cells were treated with Sal for 1h and then stained with JC-1. Red (polarized) and green (depolarized) fluorescence was measured by flow cytometery and their respective percentages were calculated. Data are presented as mean ± s.d., n = 3 from duplicates.
(F) Dose-response curves of HMLE-shEcad (purple, EMT) and HMLE-shGFP (blue, non-EMT) breast cells treated with paclitaxel. MTT assay was performed after 72 hours of treatment. Data are presented as mean ± s.d., n = 3 from quadruplicates.
(G) Levels of Sal (nM) in the lysates of HMLE-pBp and HMLE-Twist. Quantification was performed by LC-MS /MS of Sal in cell lysates, 24 hours after incubation with 5μM Sal. Data are presented as mean ± s.d. and are based on three independent experiments (biological replicates), and six independent measurements of triplicates.

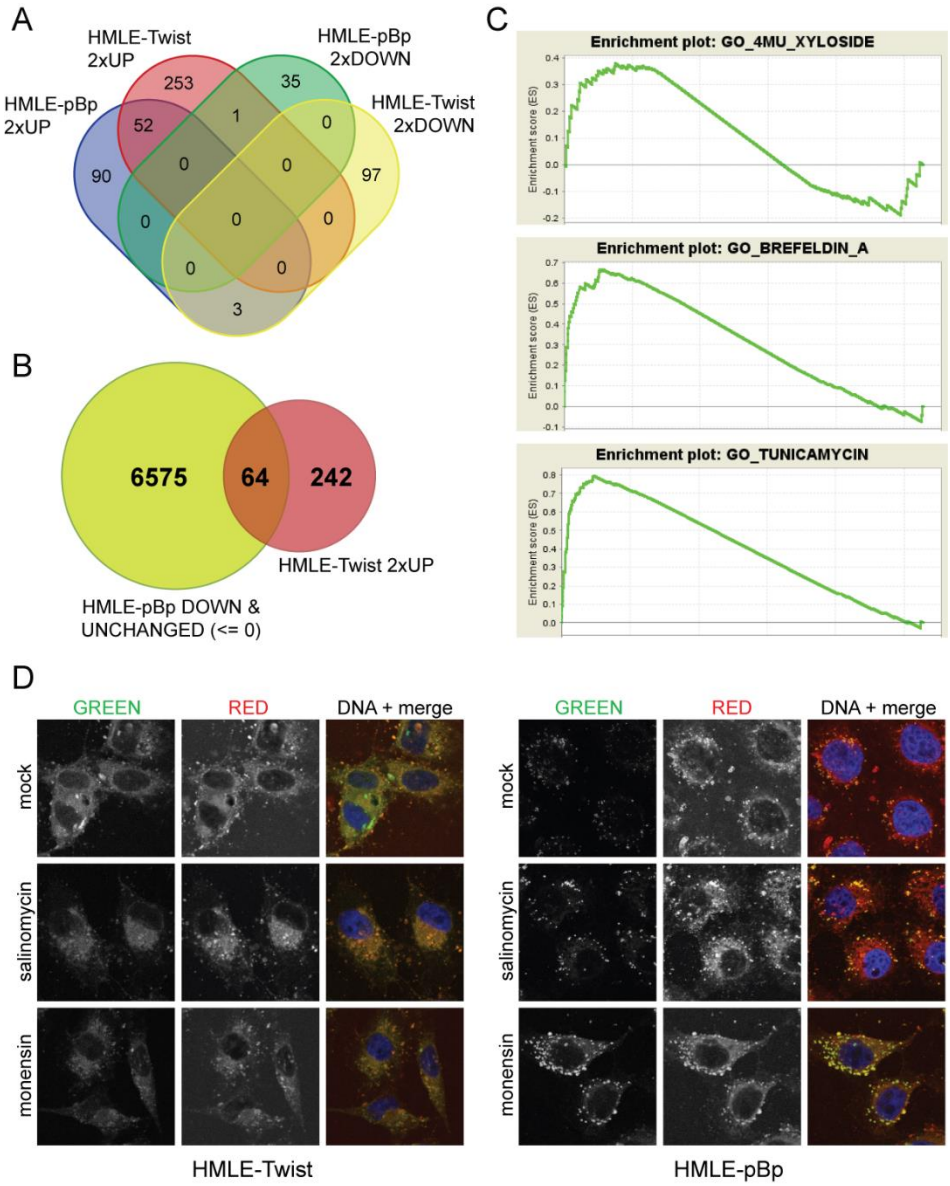

Figure S2. Differential gene expression, gene ontology and GSEA analysis of RNA-seq experiment.

(A and B) HMLE-Twist and HMLE–pBp were treated with 0.2 μM salinomycin for 24 hours and RNA-seq experiment was performed. Venn diagram representation of number of differentially expressed genes is presented. Direction and threshold of fold change used for the analysis is indicated.

(C) GSEA analysis for gene sets of known Golgi (brefeldin A and 4MU-xyloside) and ER stressor (tunicamycin) on RNA-seq data from HMLE-Twist cells treated with salinomycin is presented (analysis was performed on data ordered from largest to smallest, see Methods for details about gene sets used).

(D) Salinomycin and monensin lead to accumulation of cholesterol enriched lipid droplets in non-EMT cells. Representative confocal microscopy images of HMLE-Twist and HMLE-pBp cells after treatment with salinomycin or monensin (0.2 μM) for 24 hours. Cells were stained with Nile Red and red (ex. 565 nm, em. > 635 nm) and green/yellow (ex. 488 nm, em 520-550 nm) fluorescence was collected. DNA was counterstained with DAPI (blue). Maximum projection of 4 slices is displayed.

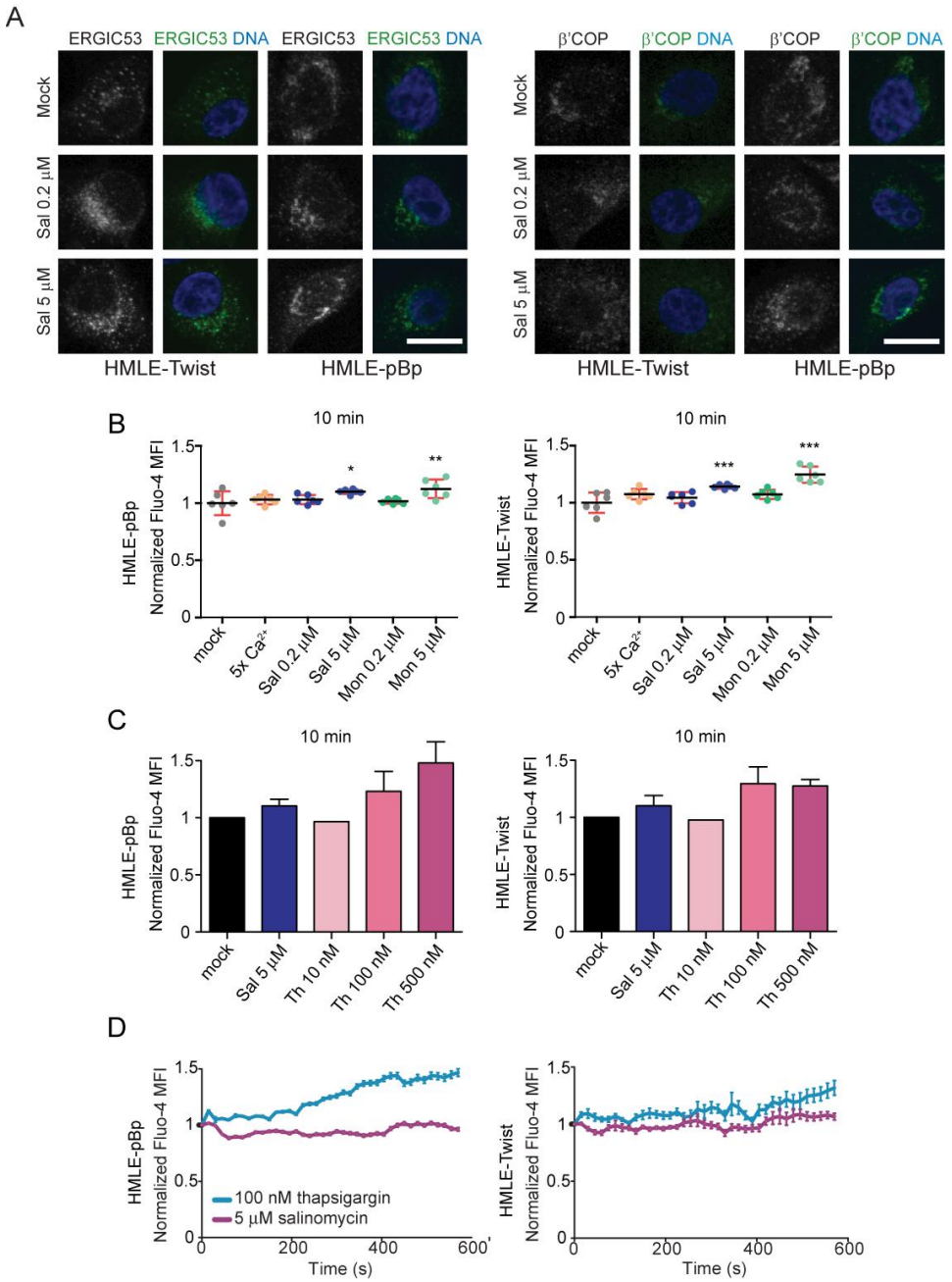

Figure S3. Salinomycin affects ER-to-Golgi compartment and does not lead to a massive depletion of ER-Ca^{2+} storage.

(A) Representative confocal microscopy images of HMLE-Twist and HMLE-pBp cells stained with anti-ERGIC and anti-β'COP primary and secondary Alexa Fluor 488 antibodies (green). DNA was counterstained with DAPI (blue). Maximum projection of 10 slices is displayed. Scale bar = 10 µm.

(B) The increase in cytosolic calcium level was monitored as an the increase in fluorescence of a Ca^{2+} specific probe (Fluo-4 AM) by flow cytometry after the addition of salinomycin (Sal), and monensin (Mon) to HMLE-pBp and HMLE-Twist cells, at the indicated concentrations. Mean ± s.d. is plotted from n = 6.

(C) The increase in cytosolic calcium level was monitored as the increase in fluorescence of a Ca^{2+} specific probe (Fluo-4 AM) by flow cytometry after the addition of salinomycin (Sal), and various concentration of thapsigargin (Th) to HMLE-pBp and HMLE-Twist cells. Mean ± s.d. is plotted from n = 3, except for Th 10 nM (n= 1) and Th 500 nM (n= 2).

(D) Live imaging of cells loaded with Fluo-4 AM. Confocal microscopy images were taken every 15 seconds, compounds were added on second 10 before acquiring second image. Mean ± s.e.m. is plotted from n = 23 cells (HMLE-pBp) or n = 11 and 9 cells (HMLE-Twist) from one experiment. One-way ANOVA with post-hoc Dunnett's multiple comparison test was used for statistical analysis (*$p < 0.05$, **$p < 0.01$, ***$p < 0.001$)

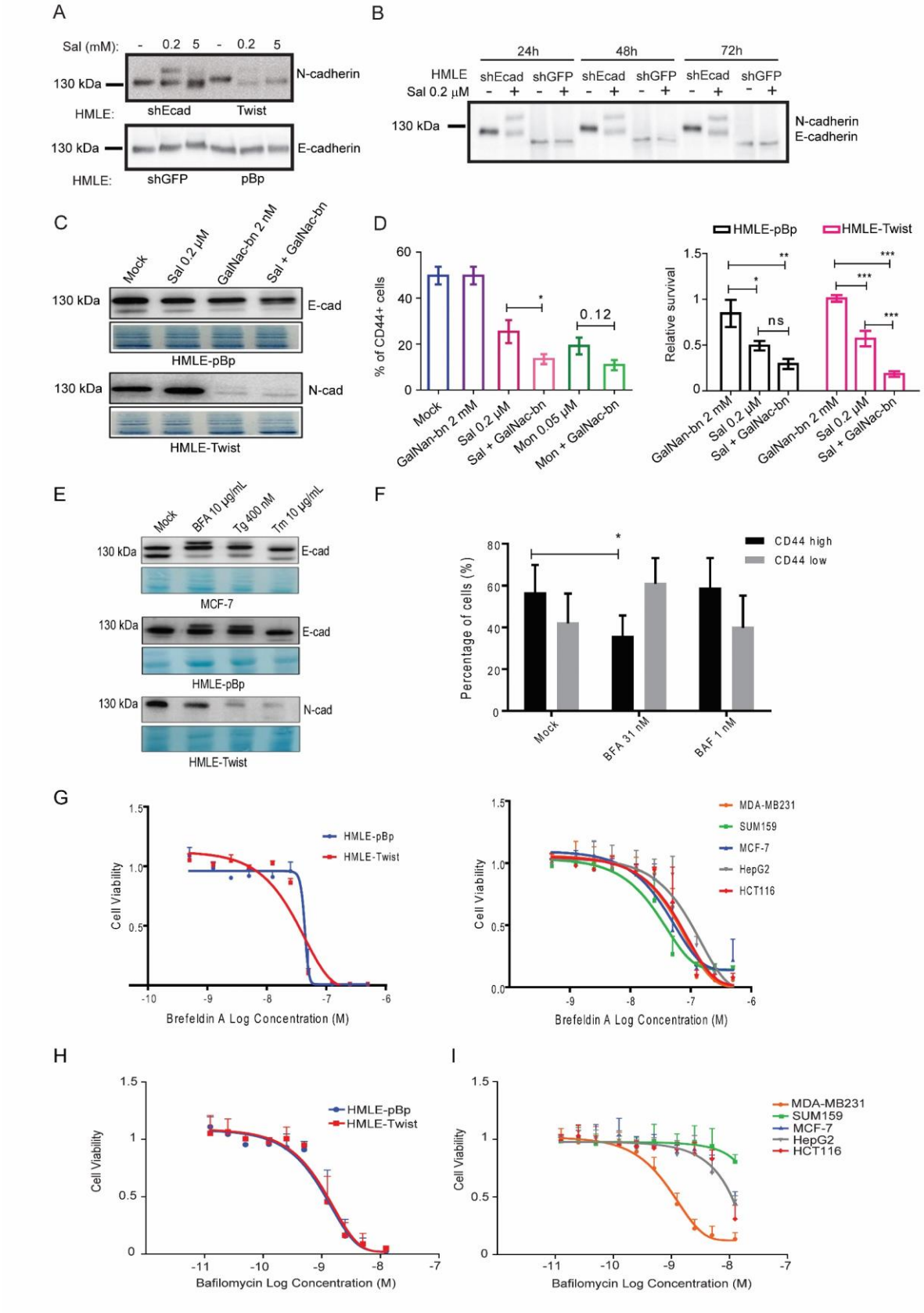
A
Sal (mM): - 0.2 5 - 0.2 5
130 kDa
N-cadherin
HMLE: shEcad Twist
130 kDa
E-cadherin
HMLE: shGFP pBp
B
24h 48h 72h
HMLE shEcad shGFP shEcad shGFP shEcad shGFP
Sal 0.2 µM - + - + - + - + - + - +
130 kDa
N-cadherin
E-cadherin
C
Mock Sal 0.2 µM GalNac-bn 2 nM Sal + GalNac-bn
130 kDa
E-cad
HMLE-pBp
130 kDa
N-cad
HMLE-Twist
D
% of CD44+ cells
0.12
Mock
GalNan-bn 2 mM
Sal 0.2 µM
Sal + GalNac-bn
Mon 0.05 µM
Mon + GalNac-bn
HMLE-pBp
HMLE-Twist
Relative survival
ns
GalNan-bn 2 mM
Sal 0.2 µM
Sal + GalNac-bn
E
Mock BFA 10 µg/mL Tg 400 nM Tm 10 µg/mL
130 kDa
E-cad
MCF-7
130 kDa
E-cad
HMLE-pBp
130 kDa
N-cad
HMLE-Twist
F
Percentage of cells (%)
CD44 high
CD44 low
Mock
BFA 31 nM
BAF 1 nM
G
Cell Viability
HMLE-pBp
HMLE-Twist
Brefeldin A Log Concentration (M)
MDA-MB231
SUM159
MCF-7
HepG2
HCT116
Brefeldin A Log Concentration (M)
H
Cell Viability
HMLE-pBp
HMLE-Twist
Bafilomycin Log Concentration (M)
I
Cell Viability
MDA-MB231
SUM159
MCF-7
HepG2
HCT116
Bafilomycin Log Concentration (M)

Figure S4. Golgi-disturbing agents selectively affect postranslational modifications of proteins and EMT-selective toxicity involves different mechanisms.
(A) The effect of the lower and higher Sal concentrations on N-cadherin processing in HMLE cellular models.
(B) Time-course western blot analysis of N- and E-cadherin after treatment with Sal in HMLE-shEcad and HMLE-shGFP cells.
(C) The effect of GalNAc(α)-O-bn (GalNac-bn) alone or in combination with 0.2 μM Sal on the processing of E- and N-cadherin in HMLE-pBp and HMLE-Twist cells. Naphtol blue staining of transferred proteins was used to evaluate equal loading.
(D) Left panel: HMLE-Twist and HMLE-pBp were seeded on day 0 at 1:1 ratio and then treated with salinomycin (Sal), monensin (Mon), GalNAc(α)-O-bn (GalNac-bn) or their combinations at indicated concentrations. Ratio of $CD44^{high}/CD44^{low}$ (EMT/non-EMT) cells after 3 days of treatment of mixed culture is shown. Data are presented as mean ± s.d., n = 3.
Right panel: Relative survival of HMLE-Twist (purple, EMT) and HMLE-pBp (black, non-EMT) cells treated with salinomycin (Sal), GalNAc(α)-O-bn (GalNac-bn) or their combination at indicated concentrations. MTT assay was performed after 72 hours of treatment. Data are presented as mean ± s.d., n = 3 from quadruplicates. One-way ANOVA with post-hoc Tukey's multiple comparison test was used for statistical analysis (*$p < 0.05$, **$p < 0.01$, ***$p < 0.001$)
(E) Western blot analysis of the effect of brefeldin A (BFA), thapsigargin (Tg) and tunicamycin (Tm) on N-cadherin and E-cadherin processing in EMT and non-EMT cells. Naphtol blue staining of transferred proteins was used to evaluate equal loading.
(F) HMLE-Twist and HMLE-pBp were seeded on day 0 at 1:1 ratio and then treated with BFA and bafilomycin A (BAF) at indicated concentrations. Percentage of CD44high/CD44low (EMT/non-EMT) cells after 3 days of treatment of mixed culture is shown. Data are presented as mean ± s.d., n = 3.
(G) Left panel: Dose-response curves of HMLE-Twist and HMLE-pBp breast cells treated with BFA.
Right panel: Dose-response curves of MCF-7, MDA-MB-231, SUM 159, HCT116 and HepG2 cells treated with BFA. MTT assay was performed after 72 hours of treatment. Data are presented as mean ± s.d., n = 3 from quadruplicates in G and H.
(H) Dose-response curves of HMLE-Twist and HMLE-pBp breast cells treated with bafilomycin A (BAF).
(I) Dose-response curves of MCF-7, MDA-MB-231, SUM 159, HCT116 and HepG2 cells treated with BAF. MTT assay was performed after 72 hours of treatment. Data are presented as mean ± s.d., n = 3 from quadruplicates.

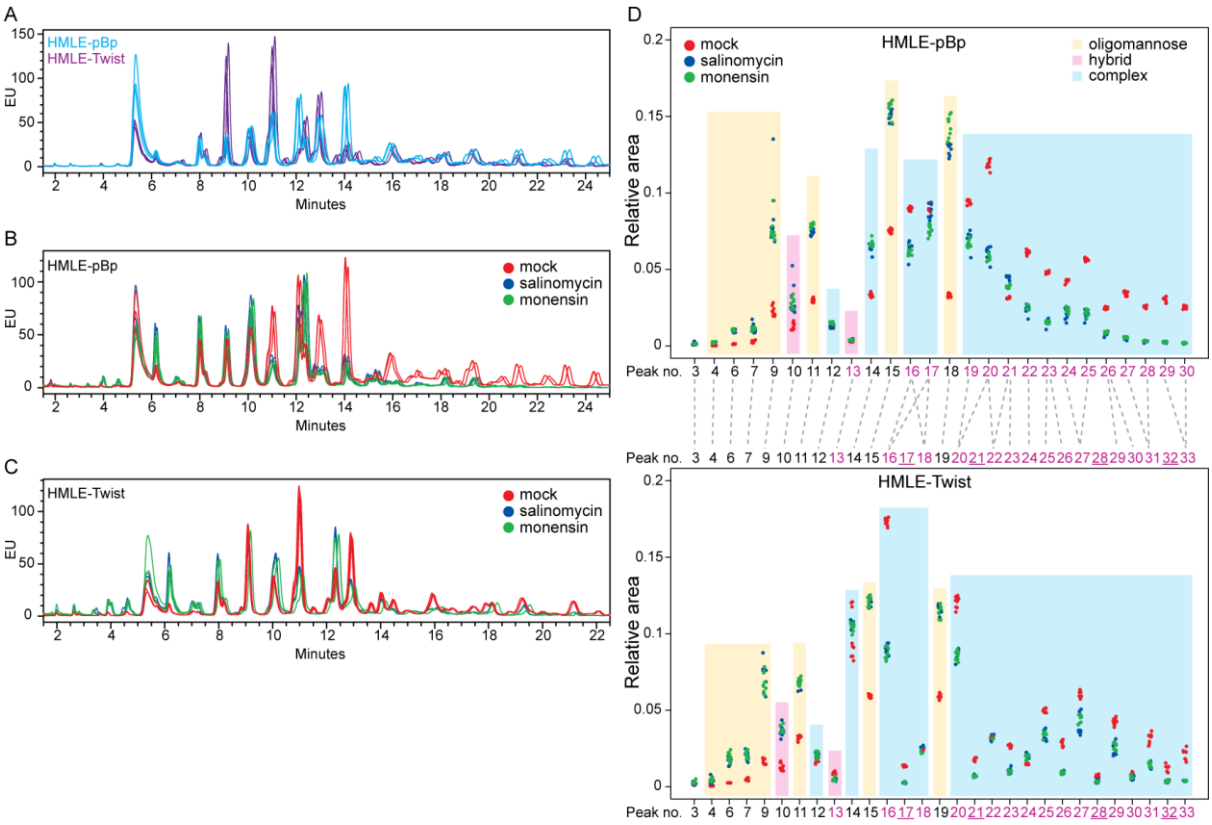

Figure S5. Salinomycin affects N-glycosylation of secreted proteins.
Overlaid chromatograms of HILIC-UPLC N-glycan profiles released from secreted proteins of mock treated EMT (HMLE-Twist) and non-EMT cells (HMLE-pBp) in (A); or mock, salinomycin and monensin treated non-EMT in (B) or EMT cells in (C). Triplicates of one representative experiment are shown in each panel.
Chromatograms in (A) were aligned by software to match the peak positions of EMT and non-EMT cells for straightforward comparison.
(D) Comparative analysis of N-glycans from secreted proteins of mock, salinomycin and monensin treated non-EMT (HMLE-pBp, upper panel) and EMT cells (HMLE-Twist, lower panel). Each area under the peak from chromatogram (B and C) was integrated and its relative amount plotted (n = 9; 3 technical replicates from each of 3 independent experiments). Peak numbers in magenta represent peaks containing sialylated glycans, underlined numbers denote peaks with sulfated/phosphorylated glycans (S/P), and grey dashed lines connect peaks containing matching major structures.

Figure S6. Blot transparency

Original blots related to Fig. 3.F

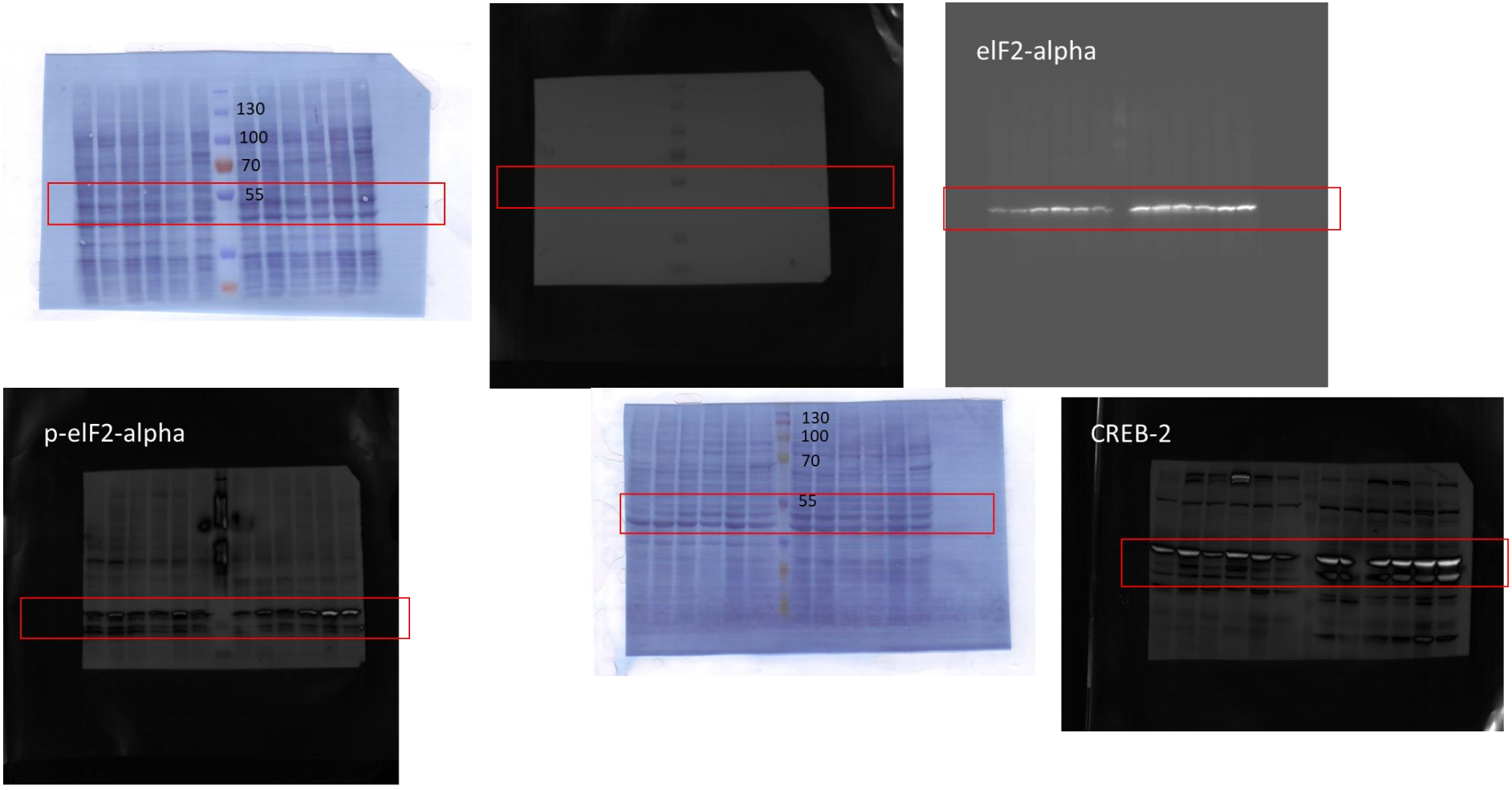

Original blots related to Fig. 4.A

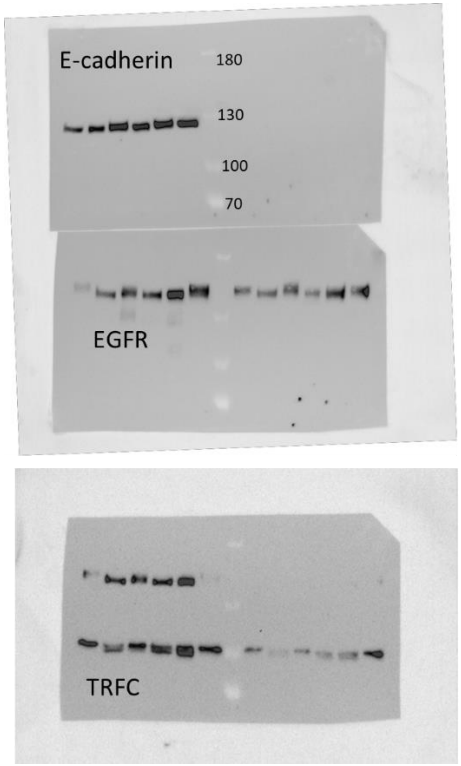

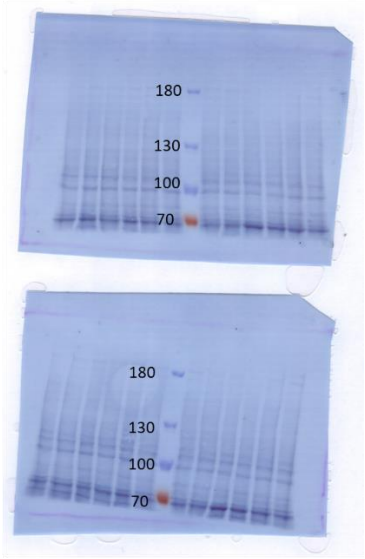

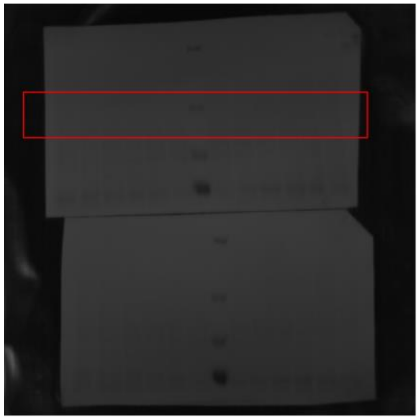

Original blots related to Fig. 4.B

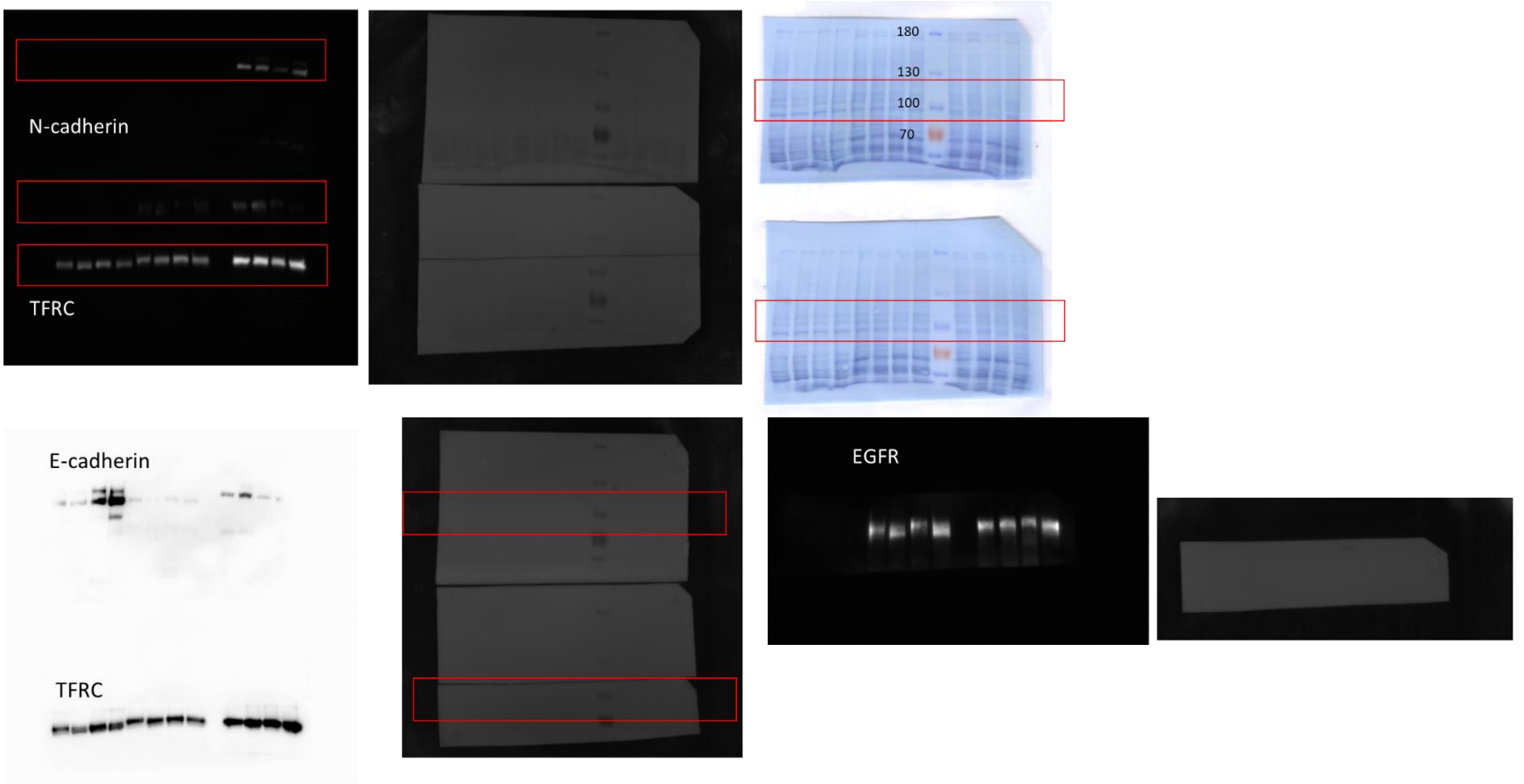

Original blots related to Fig. 4C and D.

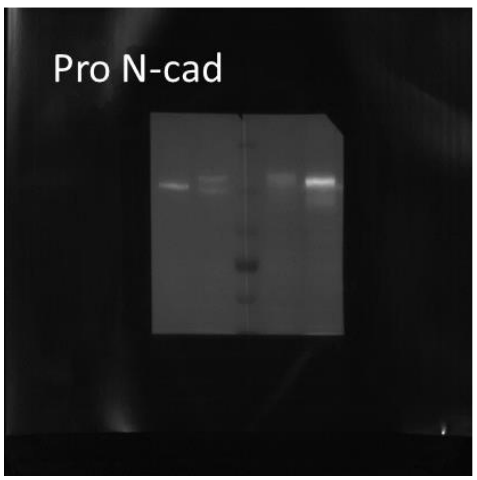

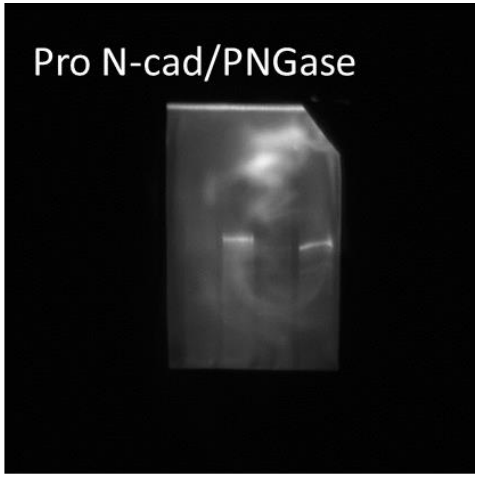

Original blots related to Fig 5A

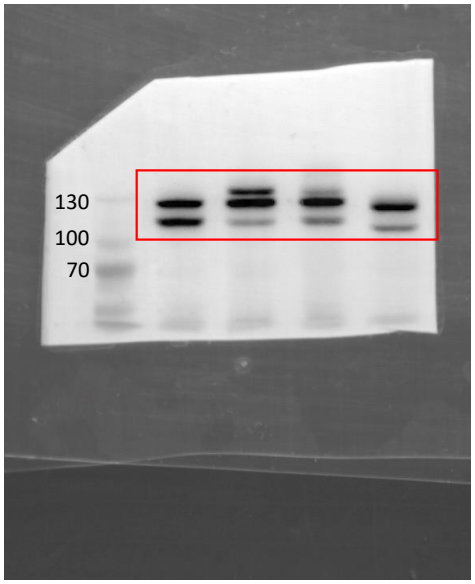

MCF-7 E-cadherin

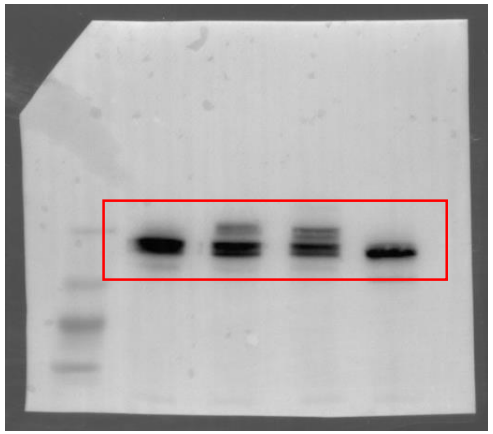

HMLE-pBp E-cadherin

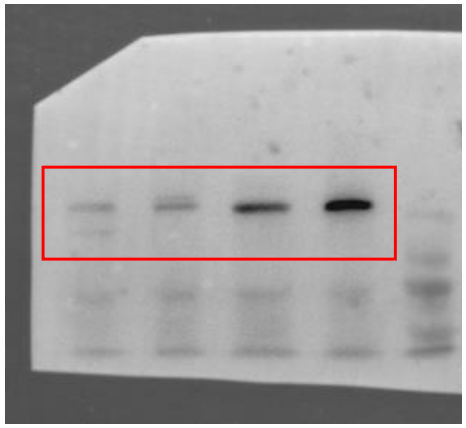

HMLE-Twist N-cadherin

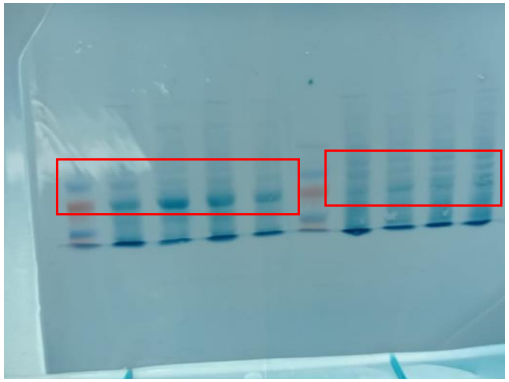

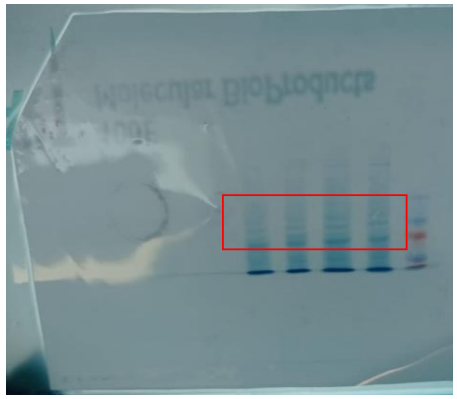

Original blots related to Fig S4C

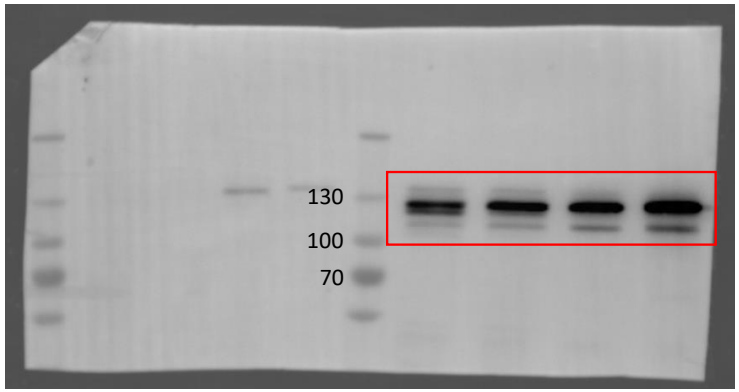

HMLE-pBp E-cadherin

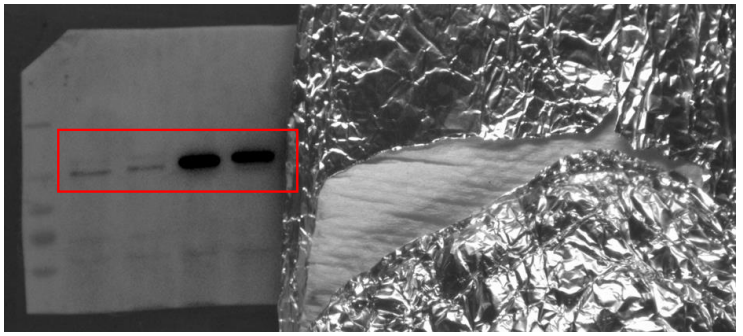

HMLE-Twist N-cad

Naphtol blue staining

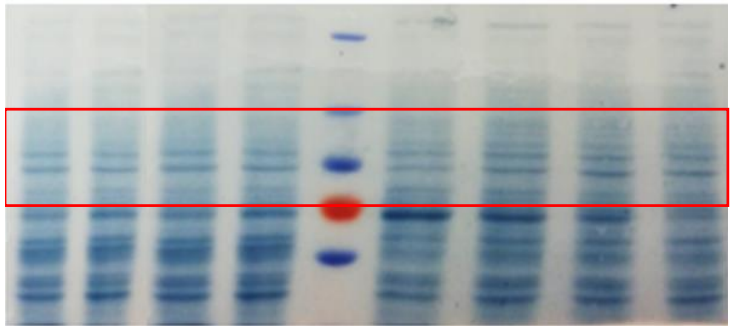

Table S1. GSEA summary table with extended information

Summary of GSEA analysis on different gene sets (ER and GA stressors or GO category) and their relation to enrichment in our experimental model (see Methods for details). * - significantly enriched; yellow - enrichment in mock treated sample, blue - enrichment in Sal treated sample. NES – normalized enrichment score, FDR – false discovery rate.

Cells	**HMLE-pBp**				**HMLE-Twist**			
Experiment	**CTRL vs. Sal**				**CTRL vs. Sal**			
Stressor or GO		*NES*	*FDR*	*p-value*		*NES*	*FDR*	*p-value*
Tunicamycin	*	-1.42	0.107	<0.01	*	-1.35	0.093	<0.01
Thapsigargin	*	-1.38	0.083	<0.01	*	-1.24	0.117	<0.01
Doxorubicin	*	1.28	0.24	<0.01		0.98	0.453	0.372
4MU-xyloside	*	-1.35	0.152	0.087		-0.97	0.526	0.569
Brefeldin A	*	-1.3	0.132	0.17	*	-1.43	0.06	<0.01
Monensin		0.82	0.762	0.611	*	-1.2	0.124	<0.01
Nigericin	*	-1.37	0.083	0.143		-0.96	0.553	0.519
HyT365	*	-1.07	0.266	0.367	*	-1.25	0.137	<0.01
Glycosylation		0.85	1	0.911	*	-1.4	0.07	<0.01

Table S2. **Differences in the relative amount of N-glycans of secreted proteins in non-EMT cells (HMLE-pBp).**

Glycan names are given in accordance with Oxford Glycobiology Institute notation: all N-glycans have core sugar sequence consisting of two N-Acetylglucosamines (GlcNAc) and three mannose residues. F in front of glycan name, indicates a core fucose α1–6 linked to the inner GlcNAc; Mx, number (x) of mannose on core GlcNAcs; Ax, number of antenna (GlcNAc) on trimannosyl core; B, bisecting GlcNAc linked β1–4 to β1–3 mannose; Gx, number of β1–4 linked galactose (G) on antenna; Sx, number (x) of N-Acetylneuraminic acids linked to galactose; S/P – sulfated/phosphorylated residue. Mean ± s.d. from n = 3 individual experiments is presented. Statistical significance was determined with one-way ANOVA with Tukey's multiple comparison post hoc test (ns – not significant, *p < 0.05, **p < 0.01, ***p < 0.001). Peaks containing only oligo-hexose sugars were eliminated from further analysis (peak numbers not present in Figure S5D and in Table below).

Peak no.	Major N-glycan	Relative integrated area (%)			ANOVA		
		mock	salinomycin	monensin	mock vs sal	mock vs mon	sal vs mon
1		n.d.	n.d.	n.d.			
2		n.d.	n.d.	n.d.			
3	FM2	0,086 ± 0,001	0,153 ± 0,077	0,135 ± 0,014	ns	ns	ns
4	M3	0,029 ± 0,004	0,212 ± 0,021	0,234 ± 0,033	***	***	ns
5		n.d.	n.d.	n.d.			
6	FM3	0,130 ± 0,014	0,977 ± 0,089	1,056 ± 0,049	***	***	ns
7	M4	0,280 ± 0,014	1,107 ± 0,263	1,123 ± 0,072	**	**	ns
8		n.d.	n.d.	n.d.			
9	M5	2,289 ± 0,188	8,383 ± 1,444	7,549 ± 0,388	**	**	ns
10	M4A1G1	1,292 ± 0,195	2,999 ± 0,819	2,793 ± 0,261	*	ns	ns
11	M6	2,991 ± 0,100	7,389 ± 0,074	7,842 ± 0,131	***	***	*
12	A2G2	1,200 ± 0,034	1,361 ± 0,083	1,505 ± 0,008	*	**	ns
13	M4A1G1S1	0,296 ± 0,012	0,376 ± 0,037	0,391 ± 0,020	*	*	ns
14	FA2G2	3,337 ± 0,088	6,450 ± 0,217	6,702 ± 0,128	***	***	ns
15	M7	7,562 ± 0,111	15,006 ± 0,229	15,570 ± 0,359	***	***	ns
16	FA2G2S1	8,986 ± 0,059	6,374 ± 0,347	6,106 ± 0,118	***	***	ns
17	FA2G2S1	8,991 ± 0,225	8,647 ± 0,546	7,588 ± 0,278	ns	*	ns
18	M8	3,320 ± 0,084	12,883 ± 0,332	14,414 ± 0,609	***	***	*
19	A2G2S2, FA2F1G2S1, FA2G2S2	9,405 ± 0,105	7,021 ± 0,369	6,665 ± 0,166	***	***	ns
20	FA2G2S2	11,825 ± 0,237	6,104 ± 0,291	5,720 ± 0,038	***	***	ns
21	FA2G2S2, FA3G3S1, A3G3S2	3,144 ± 0,053	4,416 ± 0,173	3,874 ± 0,050	***	**	**
22	A3G3S2, FA3G3S2	6,120 ± 0,062	2,417 ± 0,221	2,469 ± 0,109	***	***	ns
23	FA3G3S2	4,822 ± 0,023	1,565 ± 0,154	1,510 ± 0,059	***	***	ns
24	A3G3S3, FA3G3S3	4,261 ± 0,039	2,079 ± 0,287	2,335 ± 0,140	***	***	ns
25	FA3G3S3, FA4G4S2, A3G3S3	5,663 ± 0,065	2,044 ± 0,242	2,188 ± 0,154	***	***	ns
26	FA4G4S2	2,472 ± 0,057	0,814 ± 0,106	0,895 ± 0,050	***	***	ns
27	FA4G4S3	3,427 ± 0,121	0,499 ± 0,059	0,559 ± 0,030	***	***	ns
28	FA4G4S3	2,534 ± 0,058	0,296 ± 0,033	0,315 ± 0,004	***	***	ns
29	FA4G4S4	3,033 ± 0,138	0,238 ± 0,028	0,264 ± 0,025	***	***	ns
30	FA4G4S4	2,540 ± 0,059	0,188 ± 0,011	0,198 ± 0,009	***	***	ns

Table S3. **Differences in the relative amount of N-glycans of secreted proteins in EMT cells (HMLE-Twist).**

Glycan names are given in accordance with Oxford Glycobiology Institute notation: all N-glycans have core sugar sequence consisting of two N-Acetylglucosamines (GlcNAc) and three mannose residues. F in front of glycan name, indicates a core fucose α1–6 linked to the inner GlcNAc; Mx, number (x) of mannose on core GlcNAcs; Ax, number of antenna (GlcNAc) on trimannosyl core; B, bisecting GlcNAc linked β1–4 to β1–3 mannose; Gx, number of β1–4 linked galactose (G) on antenna; Sx, number (x) of N-Acetylneuraminic acids linked to galactose; S/P – sulfated/phosphorylated residue. Mean ± s.d. from n = 3 individual experiments is presented. Statistical significance was determined with one-way ANOVA with Tukey's multiple comparison post hoc test (ns – not significant, *p < 0.05, **p < 0.01, ***p < 0.001). Peaks containing only oligo-hexose sugars were eliminated from further analysis (peak numbers not present in Figure S5D and in Table below).

Peak no.	Major N-glycan	Relative integrated area (%; average ± s.d.)			ANOVA		
		mock	salinomycin	monensin	mock vs sal	mock vs mon	sal vs mon
1		n.d.	n.d.	n.d.			
2		n.d.	n.d.	n.d.			
3	FM2	0,117 ± 0,009	0,225 ± 0,045	0,288 ± 0,060	ns	*	ns
4	M3	0,050 ± 0,005	0,374 ± 0,123	0,427 ± 0,079	*	**	ns
5		n.d.	n.d.	n.d.			
6	FM3	0,256 ± 0,003	1,708 ± 0,198	1,960 ± 0,245	***	***	ns
7	M4, FA1	0,477 ± 0,067	1,994 ± 0,255	2,076 ± 0,203	***	***	ns
8		n.d.	n.d.	n.d.			
9	M5	1,642 ± 0,157	7,305 ± 0,738	6,835 ± 0,370	***	***	ns
10	M4A1G1	1,315 ± 0,227	3,653 ± 0,271	3,735 ± 0,074	***	***	ns
11	M6	3,195 ± 0,065	6,731 ± 0,250	6,849 ± 0,145	***	***	ns
12	A2G2	1,719 ± 0,098	2,154 ± 0,128	2,127 ± 0,125	*	*	ns
13	M4A1G1S1	0,901 ± 0,034	0,458 ± 0,024	0,479 ± 0,031	***	***	ns
14	FA2G2	9,864 ± 1,512	10,632 ± 0,122	10,443 ± 0,162	ns	ns	ns
15	M7	5,902 ± 0,082	12,103 ± 0,285	12,048 ± 0,246	***	***	ns
16	FA2G2S1	17,329 ± 0,072	8,956 ± 0,238	8,701 ± 0,322	***	***	ns
17	FA2G2S1(S/P)	1,357 ± 0,037	0,277 ± 0,028	0,261 ± 0,014	***	***	ns
18	FA2G2S1	2,383 ± 0,022	2,542 ± 0,027	2,320 ± 0,054	*	ns	**
19	M8	5,933 ± 0,107	11,543 ± 0,270	11,475 ± 0,228	***	***	ns
20	FA2G2S2	12,072 ± 0,325	8,599 ± 0,218	8,561 ± 0,262	***	***	ns
21	FA2G2S2(S/P)	1,799 ± 0,087	0,721 ± 0,029	0,696 ± 0,013	***	***	ns
22	FA3G3S1	3,309 ± 0,017	3,242 ± 0,079	3,201 ± 0,034	ns	ns	ns
23	FA3G3S1	2,670 ± 0,100	1,068 ± 0,059	0,965 ± 0,040	***	***	ns
24	FA3G3S1, A3G3S2	1,499 ± 0,041	2,054 ± 0,103	1,993 ± 0,025	***	***	ns
25	FA3G3S2	5,000 ± 0,096	3,322 ± 0,309	3,447 ± 0,096	***	***	ns
26	FA3G3S2	2,857 ± 0,167	0,923 ± 0,067	0,921 ± 0,024	***	***	ns
27	FA4G4S1, A3G3S3, FA3G3S3	5,989 ± 0,173	4,030 ± 0,625	4,398 ± 0,201	**	*	ns
28	FA3G3S3(S/P)	0,713 ± 0,057	0,343 ± 0,081	0,326 ± 0,008	**	**	ns
29	A3G3S3, FA4G4S2	4,257 ± 0,193	2,363 ± 0,361	2,634 ± 0,180	***	**	ns
30	FA4G4S2	0,847 ± 0,054	0,557 ± 0,116	0,637 ± 0,057	*	ns	ns
31	FA4G4S3	3,187 ± 0,269	1,368 ± 0,169	1,452 ± 0,105	***	***	ns
32	FA4G4S3(S/P)	1,217 ± 0,175	0,367 ± 0,043	0,352 ± 0,037	***	***	ns
33	FA4G4S4	2,146 ± 0,291	0,389 ± 0,015	0,394 ± 0,006	***	***	ns

Additional file S1 (separate file). List of selective compounds from the initial screen
(A) List of 227 EMT selective compounds from screen by Gupta et al. obtained by our modified algorithm.
(B) Selectivity of monensin and lasalocid A compared to published compounds from screen by Gupta et al. (6).

Additional file S2 (separate file). Differential expression and gene ontology analysis of RNA-seq data
HMLE-pBp cells and HMLE-Twist cells were treated with 0.2 μM Sal or mock treated.
(A and B) Analysis of ≥2 fold change differentially expressed genes in EMT and non-EMT cells after treatment with Sal.
(A) List of genes that are differentially expressed (≥ 2 fold change) in RNA-seq experiment after treatment with Sal. List is divided by Venn diagram showing overlapping and non-overlapping genes between experiments (see Figure S2A).
(B) List of 64 differentially expressed genes after Sal (≥ 2 fold change UP in EMT & unchanged or DOWN in non-EMT cells). See Figure S2B and text for more details.
(C) PANTHER overrepresentation test for biological process and cellular component GO categories on the 52 gene set (2-fold change UP in both EMT and non-EMT cells after Sal).
(D) PANTHER overrepresentation test for biological process and cellular component GO categories on the 52 gene set (≥ 2 fold change UP in EMT and non-EMT cells after Sal).
(E – G) List of biological process GO categories in EMT and non-EMT cells after treatment with Sal.
(E) List of GO categories overlapping between experimental setup's (EMT vs non-EMT, EMT vs Sal, non-EMT vs Sal).
(F) GO categories unique for Sal treated EMT cells sorted by p-value.
(G) GO categories unique for Sal treated non-EMT cells sorted by p-value.

Additional file S3 (separate file). Detected N-glycan structures
Compositions and proposed structures of N-glycans of the secreted proteins from mock, Sal and Mon (0.2 μM) treated EMT (A) and non-EMT (B) cells. Multiple N-glycan structures found within the same peak were divided into major structure (most abundant), lower abundance (~below 50% relative to the most abundant structure) and low abundance (~below 20% relative to the most abundant structure). Composition labels: N – GlcNAc, H – mannose or galactose, F – fucose, S – sialic acid and S/P – sulfated/phosphorylated residue.

Supplementary Movie 1 shows Hela cells stably expressing the trans-Golgi marker GalT-GFP (green) and H2B-mCherry incubated without treatment (control cells). Live cell imaging was performed over a 24-hour period, and images were acquired every 15 minutes.

Supplementary Movie 2 shows Hela cells stably expressing the trans-Golgi marker GalT-GFP and H2B-mCherry incubated with Sal at a concentration of 5 μM. Live cell imaging was performed over a 24 hour period and images were acquired every 15 minutes.